

## JGR Atmospheres

## RESEARCH ARTICLE

10.1029/2018JD030086

## Special Section:

Winter INvestigation of Transport, Emissions and Reactivity (WINTER)

## Key Points:

- The daytime conversion rate of  $\text{SO}_2$  to  $\text{SO}_4^{-2}$  was 0.22–0.71%/hr in winter under clear-sky conditions, with lifetimes of 140–450 hr
- For 10.5 hr of daylight, the upper limit of the oxidation rate is 16.5%/day, corresponding to a lifetime of 6.1 days
- Direct emissions of  $\text{SO}_4^{-2}$  relative to total sulfur ( $\text{SO}_2 + \text{SO}_4^{-2}$ ) had mean and median values of 1.7% and 2.8%, respectively

## Supporting Information:

- Supporting Information S1
- Data Set S1

## Correspondence to:

S. Bililign,  
Bililign@ncat.edu

## Citation:

Green, J. R., Fiddler, M. N., Holloway, J. S., Fibiger, D. L., McDuffie, E. E., Campuzano-Jost, P., et al. (2019). Rates of wintertime atmospheric  $\text{SO}_2$  oxidation based on aircraft observations during clear-sky conditions over the eastern United States. *Journal of Geophysical Research: Atmospheres*, 124, 6630–6649. <https://doi.org/10.1029/2018JD030086>

Received 30 NOV 2018

Accepted 21 APR 2019

Accepted article online 20 MAY 2019

Published online 24 JUN 2019




## Author Contributions:

**Formal analysis:** Jaime R. Green, Marc N. Fiddler, John S. Holloway, Viral Shah, Steven S. Brown  
**Resources:** Viral Shah, Steven S. Brown

**Supervision:** Jaime R. Green, Viral Shah, Steven S. Brown

**Writing - original draft:** Jaime R. Green, Marc N. Fiddler, John S. Holloway  
 (continued)

Rates of Wintertime Atmospheric  $\text{SO}_2$  Oxidation based on Aircraft Observations during Clear-Sky Conditions over the Eastern United States

Jaime R. Green<sup>1</sup> , Marc N. Fiddler<sup>2</sup> , John S. Holloway<sup>3</sup>, Dorothy L. Fibiger<sup>3,4</sup> , Erin E. McDuffie<sup>3,5,6,7</sup> , Pedro Campuzano-Jost<sup>5,6</sup> , Jason C. Schroder<sup>5,6</sup> , Jose L. Jimenez<sup>5,6</sup> , Andrew J. Weinheimer<sup>8</sup> , Janine Aquino<sup>8</sup> , D. D. Montzka<sup>8</sup> , Samuel R. Hall<sup>8</sup> , Kirk Ullmann<sup>8</sup> , Viral Shah<sup>9</sup> , Lyatt Jaeglé<sup>9</sup> , Joel A. Thornton<sup>9</sup> , Solomon Bililign<sup>10</sup> , and Steven S. Brown<sup>3</sup> 

<sup>1</sup>Applied Sciences and Technology PhD Program, North Carolina A&T State University, Greensboro, NC, USA,

<sup>2</sup>Department of Chemistry and ISET Center, North Carolina A&T State University, Greensboro, NC, USA, <sup>3</sup>Earth Systems Research Laboratory, National Oceanic and Atmospheric Administration, Boulder, CO, USA, <sup>4</sup>Now at Monitoring and Laboratory Division, California Air Resources Board, Sacramento, CA, USA, <sup>5</sup>Cooperative Institute for Research in Environmental Sciences, Boulder, CO, USA, <sup>6</sup>Department of Chemistry, University of Colorado Boulder, Boulder, CO, USA, <sup>7</sup>Now at Department of Physics and Atmospheric Science, Dalhousie University, Halifax, Nova Scotia, Canada, <sup>8</sup>National Center for Atmospheric Research, Boulder, CO, USA, <sup>9</sup>Department of Atmospheric Sciences, University of Washington, Seattle, WA, USA, <sup>10</sup>Department of Physics and ISET Center, North Carolina A&T State University, Greensboro, NC, USA

**Abstract** Sulfur dioxide ( $\text{SO}_2$ ) is emitted in large quantities from coal-burning power plants and leads to various harmful health and environmental effects. In this study, we use plume intercepts from the Wintertime INvestigation of Transport, Emission and Reactivity (WINTER) campaign to estimate the oxidation rates of  $\text{SO}_2$  under wintertime conditions and the factors that determine  $\text{SO}_2$  removal. Observations suggest that OH governs the rate  $\text{SO}_2$  oxidation in the eastern United States during winter. The range of mean oxidation rates during the day from power plants were 0.22–0.71%/hr, producing  $\text{SO}_2$  lifetimes of 13–43 days, if  $\text{SO}_2$  consumption is assumed to occur during 10.5 hr of daylight in cloudless conditions. Though most nighttime rate measurements were zero within uncertainty, there is some evidence of nighttime removal, which suggests alternate oxidation mechanisms. The fastest nighttime observed  $\text{SO}_2$  oxidation rate was  $0.25 \pm 0.07\%/hr$ , producing a combined day/night  $\text{SO}_2$  lifetime of 8.5–21 days. The upper limit of the oxidation rate (the mean +  $1\sigma$  of the fastest day and night observations) is 16.5%/day, corresponding to a lifetime of 6.1 days. The analysis also quantifies the primary emission of sulfate from power plants. The median mole percentage of  $\text{SO}_4^{-2}$  from observed plumes was 1.7% and the mean percentage sulfate was 2.8% for intercepts within 1 hr of transit to power plants. The largest value observed from close intercepts was over 7% sulfate, and the largest extrapolated value was 18%, based on intercepts further from their source and fastest observed oxidation rate.

## 1. Introduction

Atmospheric sulfate ( $\text{SO}_4^{-2}$ ) is a key component of acid deposition and tropospheric aerosols. Oxidation of  $\text{SO}_2$  is the most important source of  $\text{SO}_4^{-2}$ . Gas phase  $\text{SO}_2$  is produced mainly by fossil fuel combustion (Cullis & Hirschler, 1980; Rattigan et al., 2000), oxidation of biogenic reduced sulfur species (Aneja, 1990; Bates et al., 1992; Charlson et al., 1987), and volcanic emissions (Halmer et al., 2002; Stevenson et al., 2003). Gas-phase mechanisms for  $\text{SO}_2$  oxidation during day and night in the summer have been extensively investigated both in laboratory and in field studies (Calvert & Stockwell, 1983; Forrest et al., 1981; Forrest & Newman, 1977; Sakugawa et al., 1990). The studies are associated with a wide range of first order oxidation rates (1–6%/hr) under ambient conditions. In a more recent study, the upper limit for the  $\text{SO}_2$  to  $\text{SO}_4^{-2}$  first-order conversion rate was estimated to be 6.9 and 3.4%/hr, for coal-fired power plants in Tennessee during 1998 and 1999, respectively (Luria et al., 2001).

Direct emissions of sulfate from power stations can be in the form of either  $\text{H}_2\text{SO}_4$  or  $\text{SO}_3$ , both of which can either condense or rapidly undergo hydrolysis to make particulate  $\text{SO}_4^{-2}$  (Zaveri et al., 2010). This emission

**Writing – review & editing:** Marc N. Fiddler, John S. Holloway, Viral Shah, Steven S. Brown

contributes to the total atmospheric  $\text{SO}_4^{-2}$ . At low enough temperatures and high enough water vapor concentrations, condensed-phase concentrations of  $\text{H}_2\text{SO}_4/\text{H}_2\text{O}$  particles can be observed as a visible plume upon exit from the stack (Srivastava et al., 2004). Several studies in China have shown that dust, such as  $\text{CaSO}_4$  and other directly emitted (“primary”) forms of particulates containing  $\text{SO}_4^{-2}$ , can also impact the air and soil quality in urban and rural regions (Garland, 1977; Larssen & Carmichael, 2000; Quan et al., 2008). The direct emission of  $\text{SO}_4^{-2}$  can vary based on the age, condition, and operating temperatures of a power station, or industrial activity that relies on coalpowered boiler systems (Bahadori, 2011; Cao et al., 2010; Srivastava et al., 2004). Direct emission of  $\text{SO}_4^{-2}$  in primary biomass burning smoke has also been observed (Lewis et al., 2009).

Species such as hydrogen peroxide ( $\text{H}_2\text{O}_2$ ), ozone ( $\text{O}_3$ ), and nitrous acid ( $\text{HONO}$ ) can oxidize  $\text{SO}_2$  in the aqueous phase (Finlayson-Pitts & Pitts, 1999; Hung & Hoffmann, 2015; Rattigan et al., 2000). Liquid-phase oxidation occurs with  $\text{H}_2\text{O}_2$  at near-neutral aerosol pH, and with  $\text{O}_3$  under higher pH conditions, both of which can take place during day and night, and are faster than gas-phase oxidation rates (Davis et al., 1974; Hoffmann, 1986; Hung & Hoffmann, 2015; Sakugawa et al., 1990). Many previous field studies on atmospheric oxidation have been conducted during summertime with active photochemistry and have focused on examining the  $\text{HO}_x$  (e.g.,  $\text{OH}$  and  $\text{H}_2\text{O}_2$ ) budget in the presence of  $\text{SO}_2$  (Holland et al., 2003; Martinez et al., 2003; Ren et al., 2003; Ren et al., 2006). The aqueous  $\text{OH}$  and  $\text{H}_2\text{O}_2$  oxidation pathways, however, are much slower in cloudy and cold midlatitude winter conditions, due to low  $\text{HO}_x$  concentrations. While the heterogeneous oxidation pathways mentioned are still expected to have a larger contribution to sulfate formation than gas-phase mechanisms, several new oxidation mechanisms that have been proposed are discussed below, which could affect the rate of  $\text{SO}_2$  oxidation during winter when the more conventional mechanisms are slow.

Mineral-based aerosols that contain transition metal ions (TMIs) have been proposed to play a role in  $\text{SO}_2$  oxidation (Alexander et al., 2009; Song et al., 1970; Zhang & Carmichael, 1999), as  $\text{SO}_2$  has been observed to transform heterogeneously into  $\text{SO}_4^{-2}$  on the surface of dust particles in laboratory and modeling studies (Alexander et al., 2009; Bauer & Koch, 2005; L. Li et al., 2006; Zhang & Carmichael, 1999). The kinetics of heterogeneous oxidation of  $\text{SO}_2$  has been investigated on pure metal oxides (e.g.,  $\text{TiO}_2$ ,  $\text{Fe}_2\text{O}_3$ , and  $\text{Al}_2\text{O}_3$ ) and on mineral dust particles from the Sahara and Gobi Deserts in laboratory studies (L. Li et al., 2006; Park et al., 2017; Ullerstam et al., 2003; Usher et al., 2002). TMI catalysis pathways have been shown to be important to  $\text{SO}_2$  removal from the atmosphere on large particles (Gankanda et al., 2016; Harris et al., 2013) and clouds, second to the  $\text{H}_2\text{O}_2$  chemical pathway (Harris et al., 2013). Oxidation by TMI catalysis is less dependent on pH than oxidation by  $\text{O}_3$ . TMI from mineral dust leachate cause rapid oxidation of  $\text{SO}_2$ , which means that despite the relatively low number concentration of these particles, they can account for most of the in-cloud  $\text{SO}_2$  oxidation (Harris et al., 2012; Harris et al., 2013).

A new  $\text{SO}_4^{-2}$  formation pathway has been suggested via aqueous phase oxidation of  $\text{SO}_2$  by nitrogen dioxide ( $\text{NO}_2$ ) under foggy/cloudy conditions with high  $\text{NH}_3$  concentrations (Behera et al., 2013; Behra et al., 1989; Cheng et al., 2016). The nitrite product of the reaction can also enhance  $\text{HONO}$  formation, further promoting the particle-phase formation of  $\text{SO}_4^{-2}$  (G. Li et al., 2017; Xie et al., 2015). Aqueous oxidation of  $\text{SO}_2$  by  $\text{NO}_2$  might be an efficient sulfate formation mechanism on fine aerosols, mineral dust surfaces in the presence of high relative humidity and  $\text{NH}_3$ , and within clouds (He et al., 2014; G. Li et al., 2017; Wang et al., 2016). This  $\text{SO}_2$  oxidation process might lead to large sulfate production rates in polluted environments, leading to severe haze development (Cheng et al., 2016; Wang et al., 2016). However, this mechanism has been disputed, as aerosol pH is unlikely to be high enough, even with the large  $\text{NH}_3$  concentrations observed (Guo et al., 2017).

Calvert and Stockwell (1983) first proposed that the reactions of a Stabilized Criegee Intermediate (SCI) with  $\text{SO}_2$  could be important for production of organic acids and sulfate. CIs are produced by ozonolysis of unsaturated hydrocarbons in the atmosphere. CIs either decompose to radical species like  $\text{OH}$ , deactivate to a SCI and subsequently undergo a rearrangement reaction, or react with atmospheric species, such as  $\text{SO}_2$  to form  $\text{SO}_3$  (S. Kim, Guenther, et al., 2015; Sarwar et al., 2013; Welz et al., 2012), which is subsequently converted into  $\text{H}_2\text{SO}_4$ . Recent findings suggest that CI reactions with  $\text{SO}_2$  might account for the discrepancy between the observed and modeled concentrations of  $\text{H}_2\text{SO}_4$  during both the summer and winter (Berndt et al., 2014; Boy et al., 2013; P. S. Kim, Jacob, et al., 2015; Mauldin Iii et al., 2012; Sarwar et al., 2014).

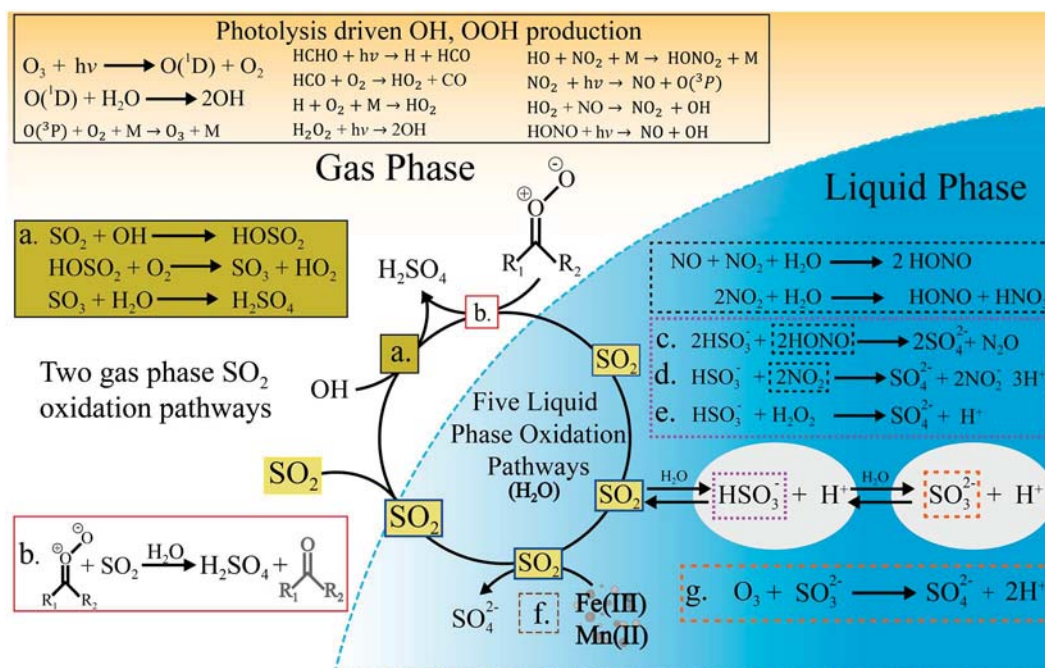


**Figure 1.** An illustrated summary of the known pathways affecting the lifetime of SO<sub>2</sub>. There are two-gas phase pathways. (a) Gaseous oxidation of SO<sub>2</sub> by OH and (b) the gas phase of oxidation of SO<sub>2</sub> by a Criegee intermediate. In the liquid phase, (c–g) reactions involve the products of SO<sub>2</sub> hydrolysis, to produce sulfate and can result in the acidification of the liquid phase.

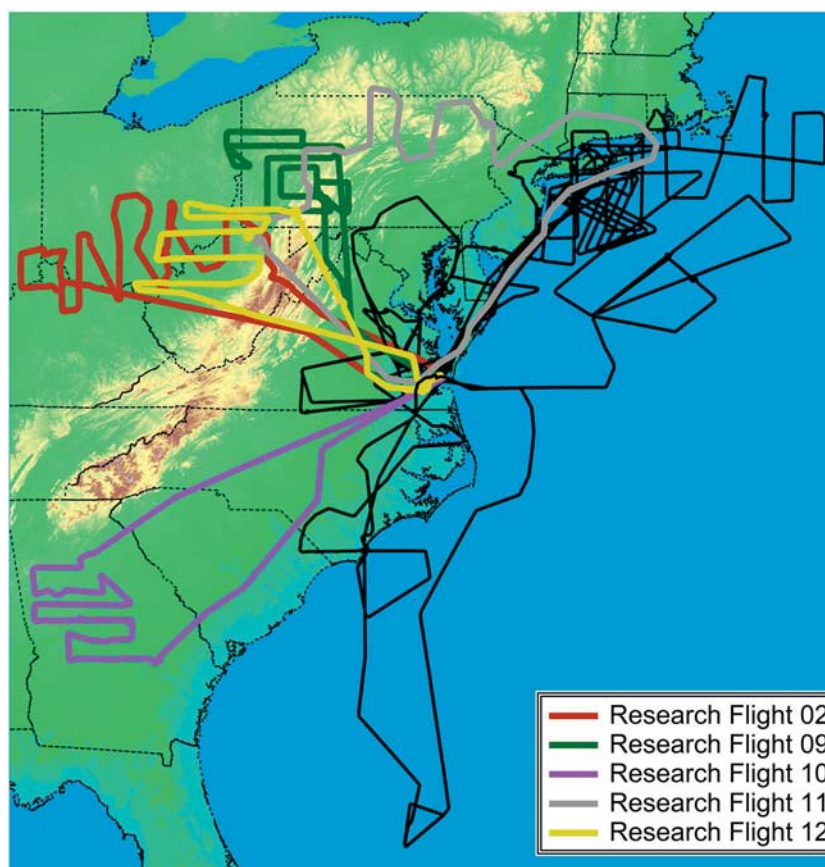
OH levels are expected to be lower in the winter due to reduced intensity and duration of sunlight and substantially lower absolute water vapor mixing ratios. Heard et al. (2004) reported maximum daily OH levels at noon ( $1.5 \times 10^6$  molecules/cm<sup>3</sup>) during January and February of 2000 in Birmingham, England; a value that is lower than those typical of summertime but still higher than expected. Box model analysis indicated that the dominant OH radical source was ozonolysis of alkene compounds and photolysis of oxygenated volatile organic compounds (VOCs; e.g., formaldehyde). In New York City during the wintertime, Ren et al. (2006) reported significantly underpredicted HO<sub>2</sub> using a photochemical box model. However, their modeled OH levels were comparable with the measurements. The dominant primary OH source in New York was HONO photolysis. Different model results with the identical observational data set of Ren et al. (2006) came to different conclusions regarding wintertime HO<sub>x</sub> budgeting, with the analysis of Cai et al. (2008) significantly underpredicting measured HO<sub>x</sub>. Schroder et al. (2018) recently quantified daytime OH in the New York City plume during the WINTER study as  $6.7 \pm 2.6 \times 10^5$  molecules/cm<sup>3</sup>, using the relative decays of multiple hydrocarbons, CO, and nitrogen oxides. This level is significantly lower than in summer studies in the same location, such as  $1.2 \times 10^6 - 3 \times 10^6$  molecules OH/cm<sup>3</sup> observed by Ren et al. (2006) but was still sufficient to form substantial amounts of secondary organic aerosols over several hours.

Figure 1 presents an overview of day and night chemistry that result in the major pathways of SO<sub>2</sub> oxidation to S(VI) forming chemical species such as SO<sub>4</sub><sup>2-</sup>. Liquid-phase oxidation is considered to occur primarily in cloud droplets (Yamagata et al., 2004).

Most studies focusing on SO<sub>2</sub> oxidation have relied on summertime data, and the rates of SO<sub>2</sub> oxidation in wintertime conditions have been based on summertime field measurements, laboratory measurements or modeled results. Examining the rate of SO<sub>2</sub> oxidation based on the data from field measurements in the winter, comparing those results with field data obtained in the summer, and quantifying observed versus expected oxidation rates might help reduce uncertainties in SO<sub>2</sub> lifetimes during the winter.

The Wintertime INvestigation of Transport, Emissions, and Reactivity (WINTER) campaign was a 6-week field campaign conducted from 6 February to 15 March 2015 on the National Science Foundation/National Center for Atmospheric Research (NSF/NCAR) C-130. Based out of National Aeronautics and Space Administration Langley in Hampton, VA, the campaign consisted of 13 research





**Figure 2.** The flight tracks used in this analysis are identified by their corresponding color. Each flight occurred on the following dates in 2015: research flight (RF) 02 on 6 February, RF 09 on 3 March, RF 10 on 7 March, RF 11 on 9 March, and RF 12 on 12 March. The flight tracks in black are the other nine flights not used in this analysis.

flights (RFs) over the eastern United States and the Atlantic Ocean, as shown in Figure 2. The area covered by this campaign allowed for observations to be made from the regions covering the Ohio River Valley, Appalachian Mountains, Virginia, New York coastal regions, the southeastern United States near Atlanta, GA, and offshore Florida. For the purposes of this study, we use four of these RFs that occurred in the north-east regions of the United States, spanning the mid-Atlantic coast to Columbus, OH, and a fifth flight in the region surrounding Atlanta, GA. These flights were selected because they sampled large sulfur emissions from coal-fired electric power generation plants and urban areas. A major goal of the WINTER 2015 campaign was to understand the wintertime oxidation rates of different trace gases including  $\text{SO}_2$ , and constrain parameters related to wintertime day and night chemistry.

## 2. Field Study and Instruments

### 2.1. WINTER Campaign Flight Description

In the WINTER campaign, 13 flights were performed using the NSF/NCAR C-130 aircraft to intercept plumes from power generating stations, point sources of pollution, regional urban and rural air, and pollution outflow over land and out to the North Atlantic.

Instruments aboard the aircraft sampled multiple primary and secondary pollutants, organic compounds, and meteorological data. Day and night flights were performed to observe both photochemistry and nighttime chemistry. Level flight legs sampled primarily within the boundary layer within an altitude range of 400 to 1,000 m above sea level. Vertical profiles were sampled outside of this altitude range through missed approaches at airports, where the aircraft descended to near ground level and then ascended to 1,500 to 2,000 m above sea level. Missed approaches reached about 10 to 100 m above the runway, and the resulting vertical

profiles were used to characterize the depth and distribution of pollutants within the boundary layer. Average temperatures for each flight ranged from -7 to 3°C.

## 2.2. Instrumentation

A modified, rack mounted TECO Model 43C Pulsed Fluorescence SO<sub>2</sub> Analyzer was deployed on the C-130 aircraft during the WINTER campaign (Ryerson et al., 1998). Sample collection took place from a downward facing inlet located on the underside and center of the C-130 fuselage. The Teflon sample delivery lines were routed through a temperature-controlled manifold regulated within a temperature range of 40–45°C to minimize SO<sub>2</sub> adsorption and desorption to and from the walls of the inlet and transfer tubing. The TECO SO<sub>2</sub> analyzer had the following modifications: an extended optical bench was used to reduce the optical background interference, a 1,000-W power supply, and a wide bore capillary was installed following the removal of the hydrocarbon kicker filtration system to allow for a flow of 2.1 L/min. The higher air flow was needed to prevent deposition or adsorption of gaseous SO<sub>2</sub> onto the internal parts of the sample delivery system and to allow for a faster time response to concentration changes. The instrument is sometimes operated with a hydrocarbon “kicker” system that removes interference from VOCs in the SO<sub>2</sub> measurement. For aircraft sampling that is not close to large, local sources of VOCs at ground level, the hydrocarbon kicker was removed to increased sensitivity and air flow through the system. The data collection frequency was 1 Hz. The TECO SO<sub>2</sub> analyzer had an automated signal calibration cycle of 1 min every 20 min of continuous operation using a 10.0 ppmv SO<sub>2</sub> in N<sub>2</sub> standard. The limit of detection of the TECO SO<sub>2</sub> analyzer was 3% ± 0.5 ppbv during measurement.

Data for other chemical species were provided from additional on-board instrumentation. Oxides of nitrogen, NO<sub>x</sub> (NO + NO<sub>2</sub>), total reactive nitrogen, NO<sub>y</sub>, and ozone, O<sub>3</sub> were measured by a six-channel cavity ring-down spectrometer (Brown et al., 2017; Wagner et al., 2013; Wild et al., 2014), a thermal dissociation laser induced fluorescence (TD-LIF) instrument (Day et al., 2002; Thornton et al., 2000), and a chemiluminescence instrument (Campos et al., 2006). The limit of detection for the direct detection of NO<sub>2</sub> specific to the WINTER campaign is 70 pptv with a 5% uncertainty for the 405-nm (cavity ring-down spectrometer) channel, while the other detection channels convert O<sub>3</sub>, NO<sub>x</sub>, and NO<sub>y</sub> to NO<sub>2</sub> for detection (Brown et al., 2017; Wild et al., 2014) with accuracies of 4–12%. The TD-LIF had a NO<sub>2</sub> detection limit of 20 pptv with a 10% uncertainty. The chemiluminescence instrument had a detection limit of 0.1 ppbv with a 0.5% uncertainty for O<sub>3</sub>, 15 ppbv with a 5% uncertainty for NO, and 25 pptv with a 25% uncertainty for NO<sub>y</sub> (Weinheimer et al., 1994). The HIAPER Atmospheric Radiation Package (HARP) measured actinic flux and photochemical rates of various photochemical processes (Laursen et al., 2006; Shetter & Müller, 1999). Aerosol sulfate measurements for particles < 1 µm in diameter were provided by a high-resolution time-of-flight aerosol mass spectrometer (HR-ToF-AMS), and HNO<sub>3</sub> measurements were provided by an iodide time-of-flight chemical ionization mass spectrometer (I-ToF CIMS). The AMS detection limit for sulfate was 137 ng/sm<sup>3</sup> (sm<sup>3</sup> = standard cubic meter at 1 atm and 273.15 K; DeCarlo et al., 2006; Dunlea et al., 2009; B. H. Lee et al., 2014; Schroder et al., 2018). The AMS collection efficiency, which varied between 0.5 for (NH<sub>4</sub>)<sub>2</sub>SO<sub>4</sub> and 1.0 for H<sub>2</sub>SO<sub>4</sub>, was determined using the parameterization of Middlebrook et al. (2012), and was applied to the 1-s data. The ToF-CIMS detection limits for the HNO<sub>3</sub> measurements were 40 ng/sm<sup>3</sup> (Lee et al., 2014). Volatile organic compounds were measured by the TOGA instrument (Apel et al., 2015). Rate constants used in our analysis were derived from several sources and are indicated in their discussion below (Atkinson et al., 2004; Burkholder et al., 2015; Manion et al., 2015; Sander et al., 2006). The WINTER campaign flight plans for all 13 RFs are depicted in Figure 2 to show the regions sampled during WINTER. RFs 02, 09, 11, and 12 cover areas in the Ohio River valley, Appalachian Mountains, and over urban regions in Pennsylvania and Ohio. RF 10 flew over Georgia, the city of Atlanta, and the surrounding urban regions.

## 2.3. Pollution Plume Identification, Tracking, and Analysis

Sulfur containing plumes were identified by increases in the signals in the measured SO<sub>2</sub> above background, which was typically 2–3 ppbv in the boundary layer for the flights in Figure 2. Analysis of the data from each individual plume was made with the goal to quantify the SO<sub>2</sub> oxidation rate from individual point sources sampled during WINTER. The following steps were used.

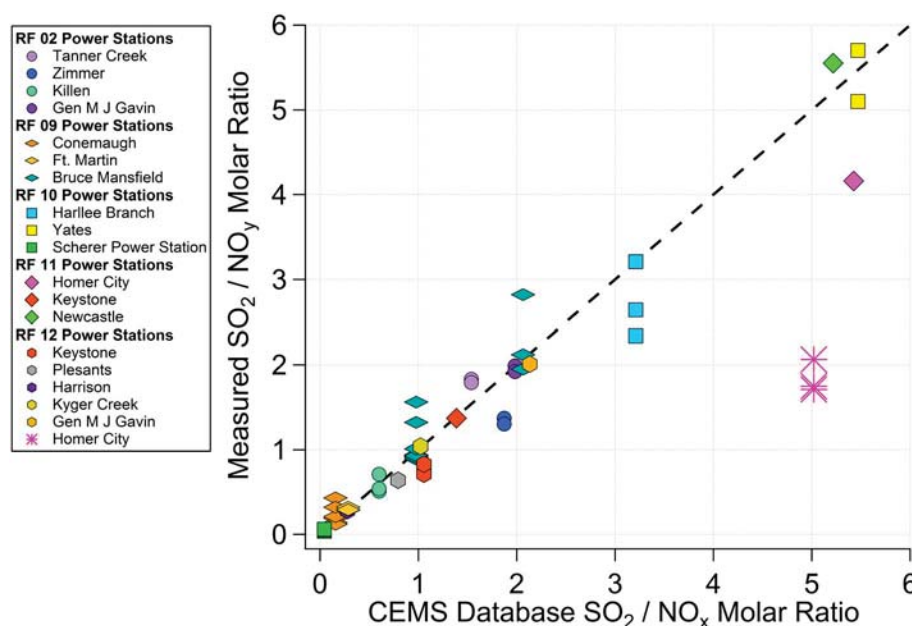


**Figure 3.** Molar ratio of  $\text{SO}_2/\text{NO}_x$  plotted against measured  $\text{SO}_2/\text{NO}_y$  ratios in plumes identified from research flights 02 and 09–12. A marker depicts each power station used in this plot. The correlation indicates positive identification and agreement between aircraft measurements and EPA continuous emission monitoring (CEMS) measurements for the plumes selected here. Multiple points for the same power station represent multiple samples made with the aircraft.

1. Composite data streams with 1-s time resolution were made for  $\text{NO}_x$ ,  $\text{NO}_y$ , and  $\text{O}_3$  to fill in data gaps produced when instruments underwent calibration cycles; typically, every 20 min of continuous operation. The procedure for this is discussed in the supporting information.
2. Scatter plots were made of the molar ratios of the following chemical species:  $\text{SO}_2$  versus  $\text{NO}_y$ ,  $\text{NO}_x$  versus  $\text{NO}_y$ ,  $\text{CO}$  versus  $\text{NO}_y$ ,  $\text{HNO}_3$  versus  $\text{NO}_y$ , and particulate sulfate versus  $\text{SO}_2$  (in concentration units of  $\mu\text{g}$  sulfur/ $\text{sm}^3$  [standard cubic meter]). Orthogonal distance regression (ODR) fitting was performed on  $\text{SO}_2$  versus  $\text{NO}_y$ ,  $\text{CO}$  versus  $\text{NO}_y$ , and  $\text{HNO}_3$  versus  $\text{NO}_y$ , while a single-sided least squares regression was used for sulfate versus  $\text{SO}_2$  and  $\text{NO}_x$  versus  $\text{NO}_y$ . These different fitting methods were used for data quality assurance in the methods undertaken during data analysis.
3. Molar ratios of  $\text{SO}_2$  to  $\text{NO}_y$  for each intercepted plume, as determined from these fits, were compared to source emission mixing ratios using the Environmental Protection Agency (EPA) continuous emission monitoring (CEMS) database. Figure 3 shows how the comparison between measured  $\text{SO}_2$  to  $\text{NO}_y$  ratios and CEMS molar ratios of  $\text{SO}_2$  to  $\text{NO}_x$  were used for plume source identification. It is assumed that the amount of  $\text{NO}_y$  measured for each plume originated from the initial amount of  $\text{NO}_x$  emitted by the point source and includes both remaining  $\text{NO}_x$  and its reaction products. It is also assumed that  $\text{NO}_x$  is emitted as  $\text{NO}_2$  for converting between mass of  $\text{NO}_x$  (the convention for the CEMS data) and moles. These plots quantitatively show how well the measured  $\text{SO}_2/\text{NO}_y$  ratio of each plume compares to value from the CEMS emission data for a given power plant, so that a positive identification of the power station that generated each observed plume can be made.

This was not the sole criteria on which a positive source identification was made. There were cases where the origin of the plume is obvious, based on the proximity to a power plant and the magnitude of chemical species being emitted (largest  $\text{SO}_2$  or  $\text{NO}_x$  emitter, for example), but the measured  $\text{SO}_2/\text{NO}_y$  ratios did not match with those from the emission database. This was the case for some plume intercepts, where the agreement between the  $\text{SO}_2/\text{NO}_y$  measured ratios and CEMS data was not better than a factor of 2. The plumes identified from the Homer City power station, measured during flight 12 and shown in Figure 3, is an example of other criteria used to identify the power plant of origin. Similarly,  $\text{SO}_2$  to  $\text{CO}_2$  ratios could also be used as criteria for identification. Unfortunately, the  $\text{CO}_2$  measurement data were collected at a rate slower than 1 Hz, which degraded the quality of its correlation to other trace gases.

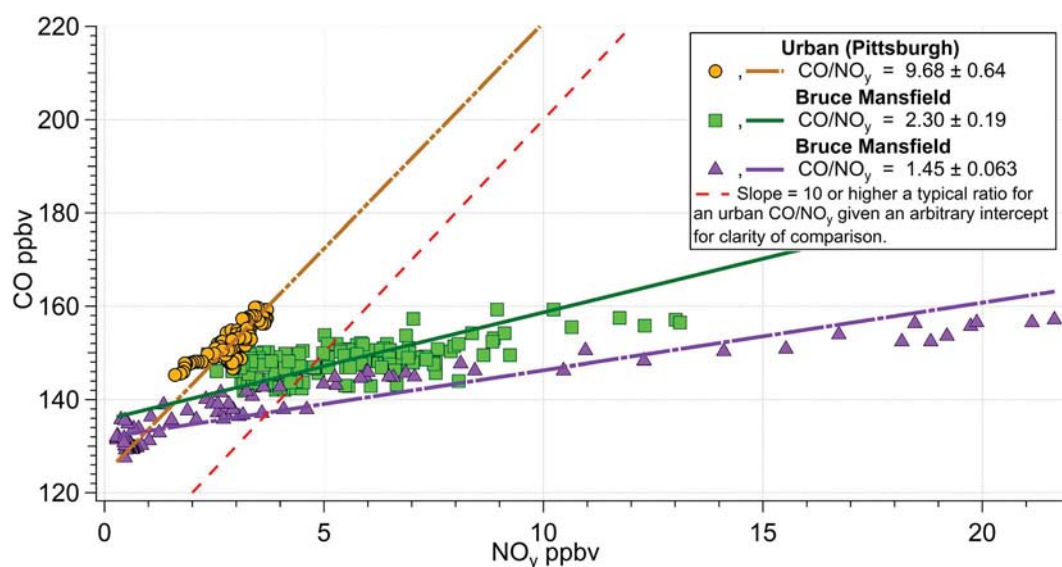


**Figure 4.** Plot of the ratio of CO/NO<sub>y</sub> from an urban plume and two power station plumes in research flight 09 on the same axis.

- For each identified plume, a Hybrid Single-Particle Lagrangian Integrated Trajectory (HYSPPLIT) back trajectory simulation was performed from the plume intercept to 8 hr prior to the intercept time.
- Three different methods were used to calculate the plume age (i.e., the time elapsed between emission and interception) for each plume. These include (1) interpolation of HYSPPLIT back trajectories, where fractional hours were derived using locations of hour markers in HYSPPLIT output and the location of the power plant (see Figure S9 in the supporting information for fractional hour derivation); (2) local wind speed as measured at the aircraft and the distance from the center of the intercepted plume to the identified source, which was applied during the daytime in well-mixed boundary layers; and (3) a chemical clock based on NO<sub>x</sub> conversion to NO<sub>y</sub> at night using the rate constant for the reaction of NO<sub>2</sub> + O<sub>3</sub> → NO<sub>3</sub> + O<sub>2</sub> (Brown et al., 2006). Further discussion is given in sections 3.1 and 3.2.
- The sulfate versus SO<sub>2</sub> slope was used to calculate the fraction of SO<sub>2</sub> in total sulfur as a function of the different transport times from step 5.
- Although narrow plumes with high concentration of SO<sub>2</sub> were often identified as originating from a single coal-fired electric power generation source, there were numerous plumes that were more diffuse and with a lower maximum SO<sub>2</sub> mixing ratio that were more likely due to urban emissions. Such emissions could be identified by their CO/NO<sub>y</sub> ratios, since urban sources generally emit larger amounts of CO relative to other pollutants than electric power generation sources. Recent inventories suggest that the urban CO/NO<sub>y</sub> ratio lies in the range 5–15 ppbv/ppbv (McDonald et al., 2013; Parrish et al., 2002; Pollack et al., 2012; Wallace et al., 2012). This ratio was used to distinguish urban plumes from electric power generation plumes, as shown in Figure 4. Each plume ratio is the slope of its correlation plots, and the ratio's error is the standard deviation of the slope retrieved by the fitting algorithm. Previous studies have suggested that a CO/NO<sub>y</sub> ratio of 10:1 or greater indicates the presence of an urban plume where light-duty traffic and diesel vehicles operate during peak operating hours. Ratios ranging from 10:1 to 4:1 indicate urban plumes that are dominated by off hour light traffic (Hassler et al., 2016; McDonald et al., 2013). Lower than 4:1 indicates a plume from power plant emissions, as power plants normally generate low mixing ratios of CO relative to CO<sub>2</sub> due to their very high combustion temperatures (Cao et al., 2010).

#### 2.4. Description of SO<sub>2</sub> Conversion to Sulfate Over Time

Equation (1) describes the conversion of SO<sub>2</sub> to sulfate, from a point source or area source for a given amount of SO<sub>2</sub> at the emission source. However, the emission may also contain a fraction of primary SO<sub>4</sub><sup>-2</sup> or a sulfur compound such as SO<sub>3</sub> that would rapidly react at or near the point of emission to produce sulfate. Plots of SO<sub>4</sub><sup>-2</sup> versus SO<sub>2</sub> were used to calculate  $\phi$ , which is the mole fraction of SO<sub>2</sub> in total sulfur, for each plume, as



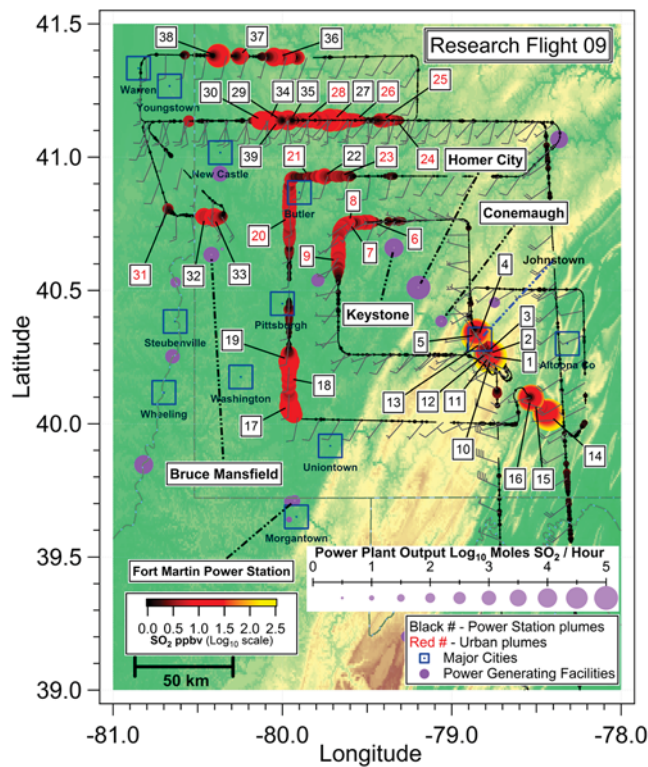


**Figure 5.** Flight track of the C-130 during research flight 09 on 3 March 2015, color and size coded by measured  $\text{SO}_2$  mixing ratio, as shown in the color bar (sizing for flight track  $\text{SO}_2$  not shown). Research flight 09 sampled the region on the southwestern corner of PA, bordering WV, MD, and OH at night. The purple dots represent the location of coal-fired electric power generation stations, sized by  $\text{SO}_2$  emissions from the continuous emission monitoring database on a  $\text{Log}_{10}$  scale, as shown in the legend. Labels indicate names of power stations positively identified as plume intercepts. Open squares indicate urban areas. Background shading indicates terrain elevation.

shown in equation (1). The error in  $\phi$  (the standard deviation,  $\sigma_\phi$ ) is derived from the slope ( $\alpha$ ) and standard deviation of the slope ( $\sigma_\alpha$ ), produced from the regression of  $\text{SO}_4^{-2}$  versus  $\text{SO}_2$  plots, as shown in equation (2). Values of  $\phi$  plotted against transit time for plumes associated with a single point source were used to calculate the oxidation rate of  $\text{SO}_2$  over time. Equation (3) (see full derivation in the supporting information) assumes first-order kinetics, with respect to  $\text{SO}_2$  using the expression  $\phi = \phi_0 e^{-kt}$  and approximating the exponential as a linear function for small values of  $kt$ .

$$\phi = \frac{[\text{SO}_2]}{[\text{SO}_2] + [\text{SO}_4^{-2}]} = \frac{1}{1 + [\text{SO}_4^{-2}]/[\text{SO}_2]} \quad (1)$$

$$\sigma_\phi \approx \frac{\sigma_\alpha}{(1 + \alpha)^2} \quad (2)$$

$$\phi = \phi_0(1 - kt) \quad (3)$$

where  $\phi_0 = \phi(0) = \frac{[\text{SO}_2]_i}{[\text{SO}_4^{-2}]_i + [\text{SO}_2]_i}$  and  $\phi(t) = \frac{[\text{SO}_2]_t}{[\text{SO}_4^{-2}]_t + [\text{SO}_2]_t}$

Plotting  $\text{SO}_4^{-2}$  against  $\text{SO}_2$  for each plume that originates from the same point source retains the mass balance of  $\text{SO}_4^{-2}$  and  $\text{SO}_2$  along the path of transport. A curve fit of the plot of  $\phi$  versus time provides an intercept that will equal  $\phi_0$  and a slope equal to  $-k\phi_0$  from equation (3). The fraction of the sulfur emission present as primary sulfate (rather than  $\text{SO}_2$ ) is given by  $\phi_0$ . The slope  $-k\phi_0$ , is the rate of  $\text{SO}_2$  loss due to oxidation.

### 3. Results and Discussion

Data from RFs 02, 09, 10, 11, and 12 (flight tracks and dates given in Figure 2) occurred in clear-sky conditions and sampled plumes from multiple large  $\text{SO}_2$  sources. Maps for each respective flight are in Figures 5 and S4–S7 in consecutive order. In these figures, the average power plant output (moles  $\text{SO}_2$ /hr) was obtained from the first quarter of 2015 from the EPA air markets program (CEMS data referred to above), and the size of the power plant marker is logarithmically scaled to this emission rate, as

seen in the legend. Where possible, time-dependent plume evolution was analyzed from multiple intercepts of plumes downwind of well-defined sources. However, both the source identification and the tracking of downwind plumes proved challenging in some cases.

It is also worth noting that the WINTER RFs sampled a wide geographic range from north to south, with the warmest temperatures encountered in plumes from power plants in the Atlanta, Georgia area. Despite the difference in wintertime conditions between the northern and southern regions of the WINTER domain, we analyze all plumes in terms of daytime versus nighttime differences only, in part due to the small number of power plant plumes in the southern part of the domain.

Missed approaches to airfields were used to ascertain the altitude of the boundary layer and to sample at lower altitudes. Several missed approaches are shown during night flights for western Pennsylvania (RF 09; Figure S1) and Atlanta, GA (RF 10; Figure S2). Ground altitude is taken relative to the airfield of the missed approach. Plumes were intercepted in distinct but shallow layers on both sides of each transect. During RF 09 (Figure S1), the vertical thickness of these plumes varied between  $\sim 70$  m (profile 0) and  $\sim 200$  m (profile 4), while the thickness was  $\sim 60$  m (profile 0) or less during RF 10 (Figure S2). During RF 09, plumes were intercepted during missed approaches between 23 km (plume 13 in Figure 5 from Conemaugh) and 85 km (plume 14 in Figure 5 and profile 4 in Figure S1 from Homer City) from their source. Parts of the profile in Figure S1 correspond to different power plants, but the most distinct narrow peak originates from Homer City, which was 46 km away. During RF 10, plumes were intercepted during vertical profiles even further from their source; up to 185 km from Bowen and 113 km from Harlee (see Figure S5). These observations



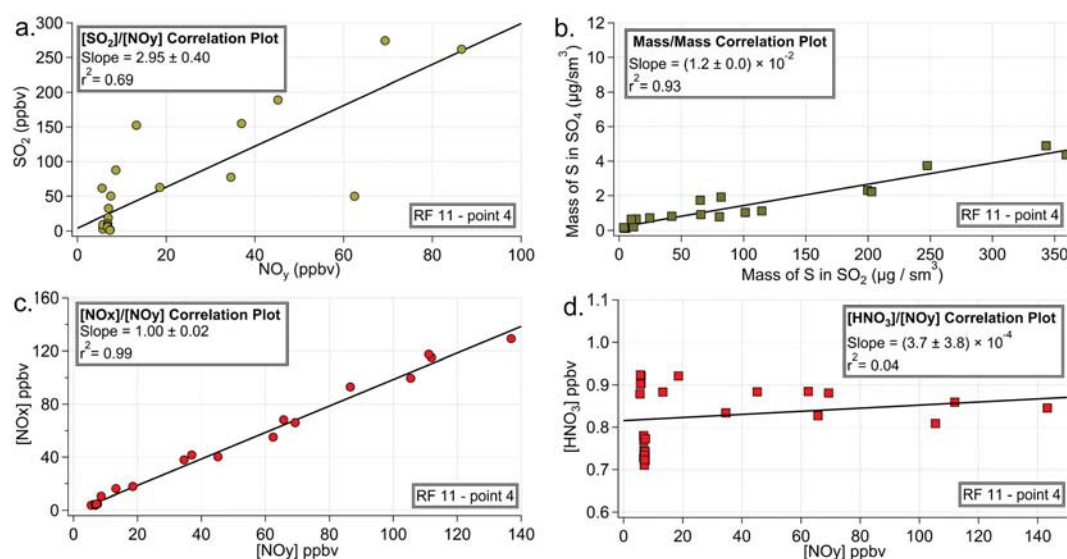


**Figure 6.** Examples of correlation plots, shown for research flight (RF) 11, plume 4. Slopes and their errors ( $1\sigma$ ) are listed in the legend along with their  $R^2$  values.

indicate that nighttime power plant plumes were widespread horizontally but confined vertically, transporting as fanning plumes (Brown et al., 2012; Fibiger et al., 2018; Fry et al., 2018; Stull, 1988). The profiles also show the  $\text{SO}_2$  plumes were situated just above the onset of a steeper gradient in potential temperature that indicates the nocturnal boundary layer. The mixing ratio of CO was enhanced below but not above the  $\text{SO}_2$  plume, and relative humidity (not shown) was high (80%) below the  $\text{SO}_2$  plume, but decreased rapidly to below 10% above it. Thus, the  $\text{SO}_2$  plumes were transported at the top of the nocturnal boundary layer and could only be sampled while vertical profiling to lower altitudes.

Plumes containing  $\text{SO}_2$ ,  $\text{NO}_x$ ,  $\text{NO}_y$ ,  $\text{O}_3$ , and  $\text{SO}_4^{-2}$  were encountered at different altitudes. There were only a limited number of sources that had plumes with multiple intercepts, despite flight plans with several legs downwind of sources. Multiple intercepts of plumes from the same source allow for the determination of the rates of chemical transformation more easily than using single intercepts from multiple sources. Only data linked to Killen/J. M. Gavin (RF 02), Bruce Mansfield (RF 09), Conemaugh (RF 09), Harlee Branch (RF 10), Scherer (RF 10), Homer City (RF 12), and Keystone (RF 12) power stations contained sets of three or more plume intercepts encountered during their respective flights. While Keystone (RF 09), Bowen (RF 10), and Yates (RF 10) had multiple intercepts, they did not have more than two data points for each due to data gaps, negative correlations between sulfate and  $\text{SO}_2$ , and chemical clocks that exceeded the time since sunset.

### 3.1. Day Flights

Examination of the daytime oxidation of  $\text{SO}_2$  used data from RF 02, RF 11, and RF 12, as shown in Figures S4, S6, and S7, respectively. Temperatures during the flights averaged  $-7.1^\circ\text{C}$  for RF 02,  $6.0^\circ\text{C}$  for RF 11, and  $4.4^\circ\text{C}$  for RF 12. Figure 6 shows an example, from plume 4 of RF 11, of several correlation plots used in this analysis. The correlation between  $\text{SO}_2$  and  $\text{NO}_y$  was generally good, with average regression slope relative standard deviations (RSDs) better than 6% for RF 12 and 9–10% for RF 02 and 11. The regression of the mass of sulfur in sulfate versus  $\text{SO}_2$  had slopes with RSDs that averaged 21% (RF 02), 15% (RF 11), and 10% (RF 12) when plumes with 4 or fewer points were excluded; which was generally of moderate precision. While high precision was found for many plumes, such as that shown in Figure 6, it was mainly limited by low sulfate concentrations. Plots of  $\text{NO}_x$  versus  $\text{NO}_y$  were more strongly correlated than for other pollutants, with average RSDs on all flights better than 1.8%. Several flights (RFs 02, 11, and 12) exhibited  $\text{NO}_x/\text{NO}_y$  ratios greater than 1, with a maximum observed  $\text{NO}_x/\text{NO}_y$  value from all flights of 1.16. When this occurred, all ratios on a flight were scaled to the maximum value (i.e., multiplied by a factor to set the largest  $\text{NO}_x/\text{NO}_y$  value equal to 1). This was not necessary for night flights. The quality of nitric acid versus  $\text{NO}_y$  data varied, largely

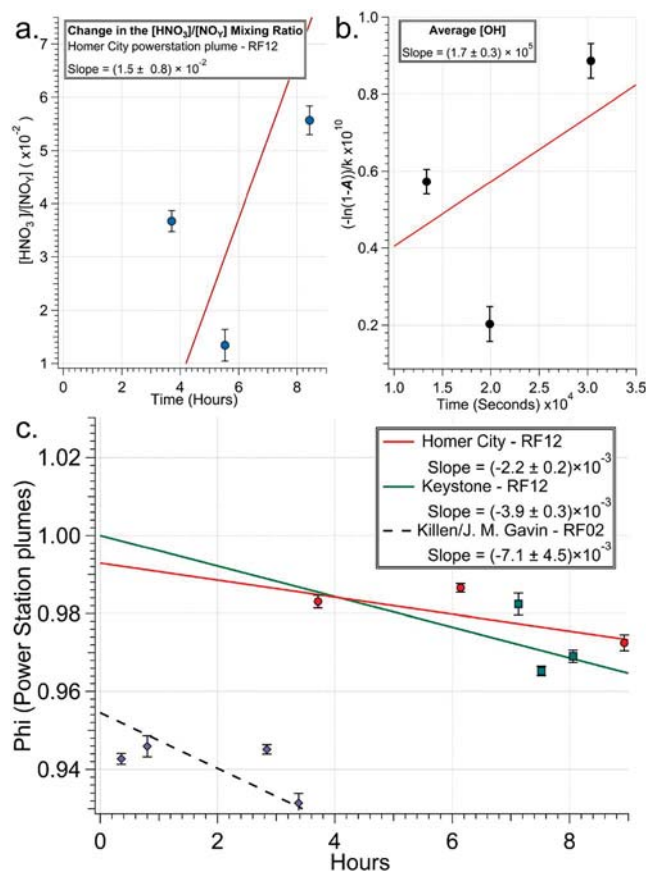


**Figure 7.** (a) A plot of multiple intercepts from Homer City Power Station (RF 12), showing  $\text{HNO}_3/\text{NO}_y$  over time. (b) A plot for determining  $[\text{OH}]$ , based on A, which is the slope of  $\text{HNO}_3/\text{NO}_y$  times the slope of  $\text{NO}_x/\text{NO}_2$ , and the transit time (see text). The  $\text{OH} + \text{NO}_2$  channel is assumed to dominate. (c) Overlaid plots of sulfur oxidation rate analysis from the daytime flights research flights (RF) 02 and 12. All graphs use weighted orthogonal distance regression fitting. The error bars are one standard deviation, derived directly from the slope fit or propagated from it using standard methods.

depending on the levels of  $\text{HNO}_3$  observed where slope RSDs averaged 45% for RF 02, 35% for RF 11, and 16% for RF 12.

Transit times from point source emissions to the point of sampling were determined as described above. Two methods were used to determine transit times, depending on the wind field, during the day. Transit times based on wind speed were used in RF 02 and 12, since the wind field was relatively uniform in speed and direction. These transit times agreed with HYSPLIT times within 1–2 hr. In RF 12, HYSPLIT back trajectories tended to curve away from the power plants, which added uncertainty to transit times using that method. HYSPLIT was used for RF 11 because the wind speed changed over the course of the flight.

Figure 7c shows plots of sulfur oxidation using equation (3) from the daytime flights, with plume intercepts attributed to the Homer City and Keystone power stations (RF 12) and Killen/Gen. J. M. Gavin power stations (RF 02). The conversion rate of  $\text{SO}_2$  to  $\text{SO}_4^{2-}$  was 0.22–0.71%/hr, based on mean slopes, which corresponds to lifetimes ranging from 140 to 450 hr. It is important to note that the intercepts for the Keystone power station were not close to the power station, and its fit was forced through one to provide a physically realistic time dependence, so that the intercept did not exceed one.

In comparison, previous studies estimated  $\text{SO}_2$  lifetimes of 4–12 hr from point sources under summertime conditions (C. Lee et al., 2011) to as long as 14 hr (Summers & Fricke, 1989). Our measurements occur over 9 hr of transport in clear-sky conditions, during which 2.0–6.4% conversion of  $\text{SO}_2$  to  $\text{SO}_4^{2-}$  is expected, based on our rate. Even using the longest summertime lifetime of 14 hr, 47% would be converted over the span of 9 hr, which would be 7.4–24 times faster than our wintertime observations. The fastest lifetime of 4 hr would result in over 89% conversion in 9 hr, which is 14–45 times faster. Previous aircraft measurements on the Cumberland power plant in Tennessee were done in midday under dry, clear-sky conditions (Luria et al., 2001). The upper limit on  $\text{SO}_2$  conversion was  $6.9 \pm 0.5\%/hr$  in late August of 1998 and  $3.4 \pm 1.2\%/hr$  in mid-July of 1999, with  $\text{SO}_2$  being only a minor sink of OH. These summer observations from a power plant are at least one order of magnitude (10 to 47 times) faster than our wintertime measurements.

The apparent  $\text{SO}_2$  oxidation rate can be compared to the  $\text{NO}_x$  oxidation rate, since the primary gas phase oxidant of both species is OH radical during the daytime. To determine the  $\text{NO}_x$  oxidation rate, the change in  $\text{NO}_x/\text{NO}_y$  ratio can be used. However,  $\text{NO}_x/\text{NO}_y$  ranged between 0.96 and 0.99 and did not decrease with plume transport time during intercepts in RF 02 and 12, so it was not useful for determining a removal rate. The  $\text{HNO}_3/\text{NO}_y$  ratio can be a proxy for the consumption of  $\text{NO}_x$ , since  $\text{HNO}_3$  is the primary photochemical product from the oxidation of reaction  $\text{NO}_2 + \text{OH}$  (Jaeglé et al., 2018; Kenagy et al., 2018), if  $\text{HNO}_3$  does not significantly partition into the condensed phase. This assumes that formation of organic nitrates and peroxyacetyl nitrate are negligible. Owing to low concentrations, TD-LIF measurements showed that nitric acid was uncorrelated with the sum of alkyl and proxynitrates, so we were unable to further constrain this assumption. Figure 7a shows the increase in the  $\text{HNO}_3/\text{NO}_y$  ratio for Homer City Power Station. Plumes from Keystone and Killen/Gen. J. M. Gavin were not included due to poor data quality or missing data caused by low  $\text{HNO}_3$  concentrations and data gaps in  $\text{HNO}_3$  measurements. The rate associated with the inclusion of particulate nitrate,  $(\text{HNO}_3 + \text{NO}_3^-)/\text{NO}_y$  versus time, produced a fit with greater uncertainty if we compare unweighted least squares; we go from an  $R^2$  of 0.317 to 0.260 when we add nitrate to nitric acid. This is due to nitrate and nitric acid measurements being uncorrelated with each other, even within individual plumes. The rate, based on  $\text{HNO}_3/\text{NO}_y$  from Homer City in RF 12, using an upper limit of 2.3%/hr and adjusting for a  $\text{NO}_x/\text{NO}_2$  ratio of 1.757 to account for conversion of NO to  $\text{NO}_2$ , an upper limit can be placed

on OH, which is  $9.9 \times 10^5$  molecules/cm<sup>3</sup>. The pressure and temperature-dependent rate constants (278 K and 943 mbar) are  $1.13 \times 10^{-11}$  cm<sup>3</sup> · molecule<sup>-1</sup> · s<sup>-1</sup> for OH + NO<sub>2</sub> and  $9.58 \times 10^{-13}$  cm<sup>3</sup> · molecule<sup>-1</sup> · s<sup>-1</sup> for OH + SO<sub>2</sub> (Atkinson et al., 2004). The SO<sub>2</sub> reaction is a factor of 11.8 slower than NO<sub>2</sub>; hence, NO<sub>2</sub> is expected to be more sensitive to OH than SO<sub>2</sub>. Using the relative rate and HNO<sub>3</sub>/NO<sub>y</sub> production rate (adjusted by the NO<sub>x</sub>/NO<sub>2</sub> ratio to  $2.7 \pm 1.40\%$ /hr), the SO<sub>2</sub> removal rate via OH is expected to be  $0.23 \pm 0.12\%$ /hr. This is commensurate with the values derived from the rate of change of the SO<sub>4</sub><sup>-2</sup> to SO<sub>2</sub> ratio during RF 12. For Homer City, the rate derived from HNO<sub>3</sub>/NO<sub>y</sub> matches the rate derived from SO<sub>4</sub><sup>-2</sup>/SO<sub>2</sub> (Figure 7c), which is  $0.22 \pm 0.02\%$ /hr. Given the agreement between both methods, the previously stated oxidation rates based on the change of the SO<sub>4</sub><sup>-2</sup> to SO<sub>2</sub> ratio represent a robust measure of SO<sub>2</sub> oxidation during the winter under cloudless conditions.

Another means of determining an average OH can be derived from HNO<sub>3</sub>/NO<sub>y</sub> and the rate of HNO<sub>3</sub> formation, which is shown in Figure 7b. This analysis assumes that HNO<sub>3</sub> is produced in a first-order process, where the first-order rate constant is equal to the product of an average [OH] and the OH + NO<sub>2</sub> second-order rate constant (Atkinson et al., 2004) and this reaction dominates NO<sub>2</sub> conversion to NO<sub>y</sub>. The integrated rate law for HNO<sub>3</sub> production can be rearranged and adjusted for NO + OH to solve for [OH], which is the slope when  $-\ln(1-A)/k$  is plotted against time, where  $A$  is  $([\text{NO}_x]/[\text{NO}_2]) \times ([\text{HNO}_3]/[\text{NO}_y])$ . While the slope error of HNO<sub>3</sub>/NO<sub>y</sub> has been propagated, NO<sub>x</sub>/NO<sub>2</sub> slope error is small ( $<2.7\%$ ) and has been neglected. The resulting OH concentration is  $(1.7 \pm 0.3) \times 10^5$  molecules/cm<sup>3</sup> for Homer City. Using previously mentioned rate constants, this would correspond to a lifetime of  $150 \pm 20$  hr and  $1700 \pm 300$  hr for NO<sub>2</sub> and SO<sub>2</sub>, respectively. Assuming NO<sub>x</sub> is initially 100% NO<sub>2</sub> and using equation (3), a pseudo-zero-order removal rate for NO<sub>x</sub> would be  $0.68 \pm 0.13\%$ /hr, which is slightly slower, but close to the NO<sub>x</sub> removal rate of  $1.5 \pm 0.8\%$ /hr based on HNO<sub>3</sub>/NO<sub>y</sub>. The corresponding SO<sub>2</sub> removal rate would be  $0.058 \pm 0.011\%$ /hr, which is still slower than the observed lower bound of the SO<sub>2</sub> removal rate at  $1\sigma$  by at least a factor of 2.9. This removal rate is statistically different than the directly measured SO<sub>2</sub> removal rate for Homer City ( $0.22 \pm 0.02\%$ /hr), having a  $t_{\text{exp}}$  of 12 in comparison to the critical  $t$  value of 4.6 for 4 degrees of freedom at 99.5% confidence.

An estimate of the OH mixing ratio can also be produced from simulations conducted with the GEOS-Chem chemical transport model for the WINTER campaign, as described by Shah et al. (2018) and Jaeglé et al. (2018). The GEOS-Chem and measurement-estimated OH were consistent for the NYC plume during WINTER RF 3 (Schroder et al., 2018). The OH mixing ratios were calculated by GEOS-Chem at 1-min resolution along the flight track. GEOS-Chem in-plume OH concentrations during RF 02 were  $(2.8 \pm 1.5) \times 10^5$  molecules/cm<sup>3</sup> for power plants,  $(4.2 \pm 2.5) \times 10^5$  molecules/cm<sup>3</sup> in urban plumes,  $(3.6 \pm 2.2) \times 10^5$  molecules/cm<sup>3</sup> for combined urban/power plant plumes. While urban plumes may have more OH in the Ohio River Valley, it is not statistically different at 95% confidence ( $t$  value of 1.6 with 24 degrees of freedom). GEOS-Chem in-plume OH concentrations were  $(1.2 \pm 0.5) \times 10^6$  molecules/cm<sup>3</sup> during RF 11 and  $(2.8 \pm 0.3) \times 10^6$  molecules/cm<sup>3</sup> during RF 12. For daytime flights, the GEOS-Chem OH bounds (smallest- $1\sigma$  to largest- $1\sigma$ ) were  $1.4 \times 10^5$  (RF 2) to  $3.1 \times 10^6$  molecules/cm<sup>3</sup> (RF 12). After adjusting for temperature and pressure for their respective flights, the expected NO<sub>x</sub> removal rate for this range of OH concentrations was 0.61-13%/hr. The expected SO<sub>2</sub> removal rate was 0.049-1.1%/hr. While the lower bound is within the observed rate for NO<sub>x</sub> removal, the upper bound is much faster than what is observed. The observed SO<sub>2</sub> removal rate is within the range predicted by GEOS-Chem, though the range is quite broad. Focusing on RF 12, GEOS-Chem predicts removal rates of 11-13%/hr for NO<sub>x</sub> and 0.86-1.1%/hr for SO<sub>2</sub>, both of which are in poor agreement with RF 12 observations. Part of this discrepancy may be due to GEOS-Chem calculating the instantaneous concentration of OH, while our measurements represent an average value of the OH concentration during transit. Given that GEOS-Chem uses the same rate constants as this work, the rate of OH removal by SO<sub>2</sub> and NO<sub>2</sub> would only depend on the concentrations of SO<sub>2</sub> and NO<sub>2</sub> for a given steady state concentration of OH. GEOS-Chem under predicted SO<sub>2</sub> and NO<sub>2</sub> by a factor of 1-4.5 (2.9 times smaller, on average) when compared to observed concentrations during RF 12. This is largely a result of mismatch between the observed and predicted locations and magnitudes of the power station plumes, the latter of which was underestimated. The smaller predicted sinks for OH may account for the higher instantaneous concentrations of OH, given that their modeled removal rates would be slower.

Lastly, OH can be estimated from measurements of anthropogenic VOCs in urban plumes using the relative rate method (Roberts et al., 1985; Schroder et al., 2018). TOGA measurements were only available in RF 02 (of the flights analyzed here), and the temporal resolution of the TOGA instrument is relatively slow compared to plume size. As such, only five plumes contained more than two (3-6) measurements. Correlation plots were made for each plume by plotting o-xylene and butenes against toluene. Temperature-dependent rate constants for the reaction of the anthropogenic volatile organic compounds (AVOC) with OH were from IUPAC for toluene (Atkinson et al., 2004), and NIST for o-xylene, isobutene, and n-butene (Manion et al., 2015); the last two of which were averaged. The concentration of OH is equal to the slope of a plot (unweighted least squares), where  $\ln([AVOC]/[toluene])/(k_{toluene}-k_{AVOC})$  for each plume is plotted against their transit time, as shown in Figure S3. Benzene was not used because it was found to have different spatio-temporal behavior than other AVOCs (Schroder et al., 2018). OH concentrations from o-xylene were  $(-1.2 \pm 9.4) \times 10^5$  molecules/cm<sup>3</sup> and  $(1.5 \pm 3.7) \times 10^5$  molecules/cm<sup>3</sup> for butenes. The uncertainty of this measure of OH is very large for this method, producing standard deviations exceeding the mean value. The most precise result was from butenes, which, if using IUPAC rate constants and the average temperature and pressure for RF 02, would produce removal rates of  $0.66 \pm 1.63\%/hr$  for NO<sub>x</sub> and  $0.054 \pm 0.134\%/hr$  for SO<sub>2</sub>. While NO<sub>2</sub> removal based on HNO<sub>3</sub>/NO<sub>y</sub> ( $0.88 \pm 1.30\%/hr$ ) closely matches this broad range, observed rates of SO<sub>2</sub> removal ( $0.22$ - $0.71\%/hr$ ) are significantly faster than what is expected from AVOC analysis.

Generally, oxidation during the day is slow in the winter for both NO<sub>x</sub> and SO<sub>2</sub>. Given that the reaction of OH with NO<sub>2</sub> is relatively fast compared to other reactions discussed in this work, NO<sub>x</sub> should be the most sensitive to the concentration of OH.  $9.9 \times 10^5$  molecules/cm<sup>3</sup> OH from HNO<sub>3</sub>/NO<sub>y</sub> can be used to constrain other estimates. This is somewhat lower than the maximum daily OH concentration of  $1.5 \times 10^6$  molecules/cm<sup>3</sup> reported by Heard et al. (2004) during the winter in Birmingham, England, though our measurements would represent average, or plume integrated values. The value from HNO<sub>3</sub> formation kinetics is  $(1.7 \pm 0.3) \times 10^5$  molecules/cm<sup>3</sup>, which falls below this upper limit and is more accurate than the direct HNO<sub>3</sub>/NO<sub>y</sub> value. GEOS-Chem largely overpredicts the estimated concentration of OH, with only RF 02 consistently falling within this upper bound. During RF 12, GEOS-Chem overestimates OH on average, by a factor of 2.8 when compared to the HNO<sub>3</sub>/NO<sub>y</sub> derived upper limit, which was determined on the same flight. This overprediction of OH is not consistent with previous assessments that show OH concentrations calculated by a different model (the Air Quality Forecast Modeling System) are significantly underestimated by a factor of 5 during the winter (Cai et al., 2008). Previous work on OH approximations during RF 11 showed good agreement between AVOC-derived OH and GEOS-Chem (Schroder et al., 2018). This is not the case in this work, as GEOS-Chem overestimates OH by approximately an order of magnitude. Among the estimates based on AVOCs, only butenes produced a reasonable result of  $(1.5 \pm 3.7) \times 10^5$  molecules/cm<sup>3</sup> OH, which was also the most precise. While some agreement is found, AVOC-based estimates of OH in this work were highly uncertain.

### 3.2. Nighttime Observations for Power Plants

RF 09, depicted in Figure 5, and RF 10, shown in Figure S5, occurred near Pittsburgh, Pennsylvania, and Atlanta, Georgia, respectively. Points labeled with black numbers have been identified as power plant plumes, while those with red numbers have been identified as originating from an urban source. Temperatures during the flights ranged between  $-10$  and  $4$  °C, with an average temperature of  $-7.8$  °C during RF 09 and  $3.7$  °C near the boundary layer during RF 10. Examples of correlation plots generated for a nighttime flight plume are given in Figure 8, for plume 38 of RF 09. Correlations for SO<sub>2</sub>/NO<sub>y</sub> were good, especially for the Pittsburgh flight, with slope RSDs averaging 7.1% for RF 09 and 19% for RF 10 for plumes with positive slopes. SO<sub>4</sub><sup>-2</sup>/SO<sub>2</sub> followed a similar trend, having an average slope RSD of 16% for RF 09 and 47% for RF 10. These RF 9 values do exclude plumes with only three data points, and the RF 10 values exclude those plumes in which a negative slope was found due to poor correlations; six for SO<sub>2</sub>/NO<sub>y</sub> and eight for SO<sub>4</sub><sup>-2</sup>/SO<sub>2</sub>, of 32 plumes. The NO<sub>x</sub>/NO<sub>y</sub> slope RSDs for both flights were better than 4.8% on average. None of these errors includes propagated instrument uncertainty. In many cases, particularly for NO<sub>x</sub> and NO<sub>y</sub> in RF 10, data gaps made interpretation difficult. RF 09 did not suffer as many breaks and data quality was generally better.



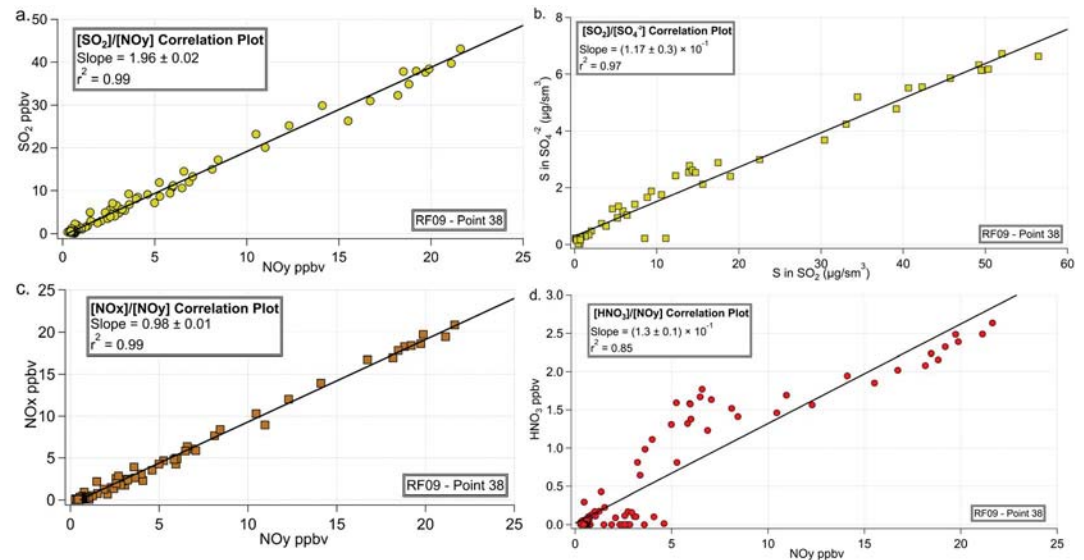


**Figure 8.** Examples of correlation plots generated from plume 38 of research flight (RF) 09.

We used the nighttime chemical conversion of  $\text{NO}_x$  to  $\text{NO}_y$  to estimate the time aloft for each of the plumes during the night, and to see the changes in sulfates versus  $\text{SO}_2$  relative to the conversion of  $\text{NO}_x$  to  $\text{NO}_y$  over time. The nighttime process that results in the conversion of  $\text{NO}_x$  to  $\text{NO}_y$  is governed by reaction of  $\text{NO}_2$  with  $\text{O}_3$ , which has a known temperature dependent rate constant (Burkholder et al., 2015). The  $\text{NO}_x/\text{NO}_y$  chemical clock has been described previously (Brown et al., 2004), and the governing equation for determining the transit time ( $t_{\text{NO}_x/\text{NO}_y}$ ) is given here, in equation (4). In this equation,  $m$  is the slope of  $\text{NO}_x$  versus  $\text{NO}_y$  from the correlation plot. Not previously presented was the propagated uncertainty in the transit time,  $\sigma_{t_{\text{NO}_x/\text{NO}_y}}$ , is given in equation (5). The time estimated by the wind speed and HYSPLIT trajectory provided some agreement within 1 hr but was not the preferred method of providing a plume transit time estimate at night. The lack of agreement between HYSPLIT back trajectories and  $\text{NO}_x$  to  $\text{NO}_y$  chemical clocks was possibly due to the difficulty in predicting nighttime wind speeds from within the model, and with the combined uncertainty of the  $\text{NO}_x$  and  $\text{NO}_y$  measurements and ODR curve fit. The combined instrumental uncertainty for each of the  $\text{NO}_x$  and  $\text{NO}_y$  measurements is 13%, which would be added to the uncertainty of the unweighted curve fit of a given plot of  $\text{NO}_x$  versus  $\text{NO}_y$ .

$$t_{\text{NO}_x/\text{NO}_y} = \frac{-\ln(m)}{2k[\text{O}_3]_{\text{avg}}} \quad (4)$$

$$\sigma_{t_{\text{NO}_x/\text{NO}_y}} \approx \left| \frac{\ln(m)}{2k[\text{O}_3]_{\text{avg}}} \right| \sqrt{\left( \frac{\sigma_m}{m \ln(m)} \right)^2 + \left( \frac{\sigma_{[\text{O}_3]}}{[\text{O}_3]_{\text{avg}}} \right)^2} \quad (5)$$

Titration of ozone was accounted for by removing points from the  $\text{NO}_x/\text{NO}_y$  fit in which  $\text{O}_3$  was significantly depleted below 20–30% of the maximum (background) value. Low ozone values were removed to minimize the RSD of the slope of the  $\text{NO}_x/\text{NO}_y$  fit. In addition to titration, all plumes were checked against the time since sunset. The time since sunset is based on the time difference between the intercept and sunset. For RF 09, this was 22:12 UTC (18:12 local) the previous day, on 2 March 2015, using Pittsburgh, PA, as the location. For RF 10, this was 22:38 UTC (18:38 local) the previous day, on 6 March 2015, using Atlanta, GA as the location. All RF 09 plumes had chemical clock times less than the time since sunset, except one, which was the same within error. Several Bruce Mansfield plumes (36 through 39) were excluded because they occurred after daybreak, when  $\text{NO}_3$  can photolyze and the nighttime clock is no longer valid. In RF 10, several

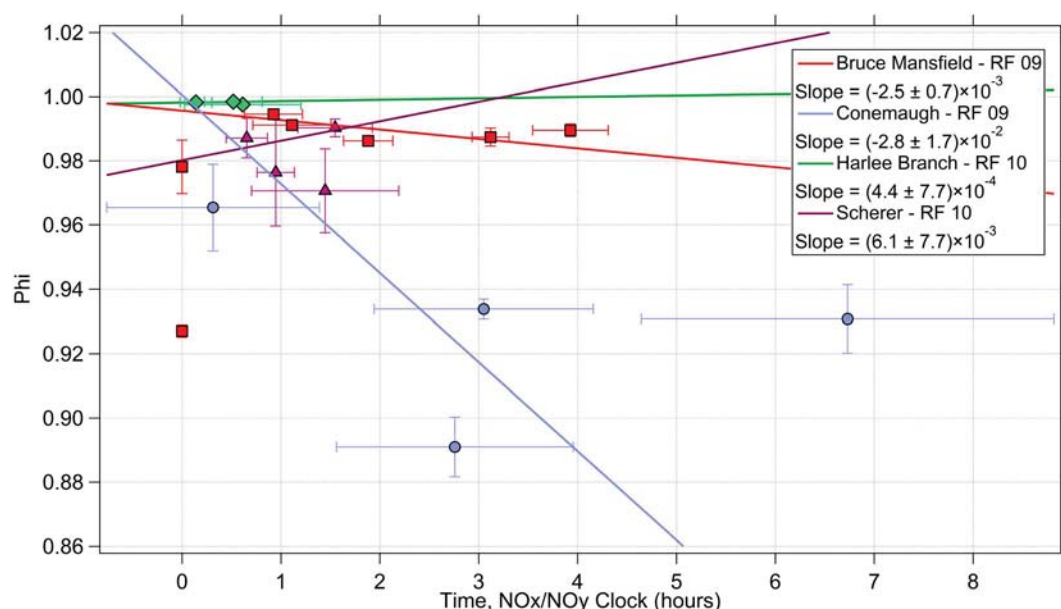


**Figure 9.** Plots for analysis of sulfur oxidation rate for power plants during nighttime flights research flight (RF) 09 and 10. The time aloft for each plume intercept is based rate of chemical conversion of  $\text{NO}_x$  to  $\text{NO}_y$  during the night, using equations (4) and (5). Each plot of  $\phi$  (labeled as Phi on the graph) versus time in hours gives the slope, which is pseudo-zero-order rate constant for of  $\text{SO}_2$  loss in  $\text{hr}^{-1}$ .

plumes, mostly associated with urban emissions, were excluded from analysis (5 of 32) because their chemical clock exceeded the time since sunset by at least 40 min.

Power plants with multiple intercepts that contained sulfur were investigated at night. Plots of  $\phi$  are presented in Figure 9 for Bruce Mansfield (RF 09), Conemaugh (RF 09), Harlee Branch (RF 10), and Scherer (RF 10). Both RF 10 power plants did not show nighttime removal rates that were different from zero within  $1\sigma$ . Conemaugh was very fast, at a rate of  $2.8 \pm 1.7\%/hr$ ; some 10 times faster than daytime oxidation. However, while its rate was different from zero within  $1\sigma$ , it was not different from zero within  $2\sigma$ . Additionally, this value is highly dependent on the fit method. Unweighted fitting, using either ODR or least squares, yields a rate of  $0.39 \pm 0.77\%/hr$ , which is zero within uncertainty. The relatively large rate and small uncertainty in the weighted ODR rate is likely an artifact of the large uncertainty of the transit time, and the rate associated with Conemaugh should be discounted. Curiously, Bruce Mansfield showed a nighttime removal rate of  $0.25 \pm 0.07\%/hr$ , which is commensurate with the daytime removal rate  $0.23\text{--}0.71\%/hr$ . While most of these nighttime plumes suggest an oxidation rate of zero, Bruce-Mansfield shows that a nighttime removal rate during the WINTER may be possible, which warrants deeper investigation into heterogeneous sulfur chemistry.

### 3.3. Nighttime Observations for Urban Areas

RFs 09 and 10 allowed an opportunity to examine emissions from the cities of Pittsburgh and Atlanta in the nighttime residual layer. In general, urban plumes were encountered at a higher altitude than plumes originating from power stations. This implies that the urban plumes were brought to this altitude by mixing processes occurring in the convective boundary layer prior to nightfall and remained at that altitude in the absence of convective mixing during the night.

Urban areas produce emissions over a relatively broad area, as opposed to power plants that can be treated as point sources. As such, HYSPLIT back trajectories and wind speed-based transit times become unreliable. The previously discussed chemical clock based on  $\text{NO}_x/\text{NO}_y$  was used for urban plumes associated with RF 09 and 10, as shown in Figure 10. Figure 10 shows that RF 09 had a significant  $\text{SO}_2$  removal rate of  $2.2 \pm 0.2\%/hr$ , while RF 10 had a rate that was not statistically different from zero (production of  $0.035 \pm 0.23\%/hr$ ). This RF 09 observation is quite rapid, being about 10 times faster than the daytime removal

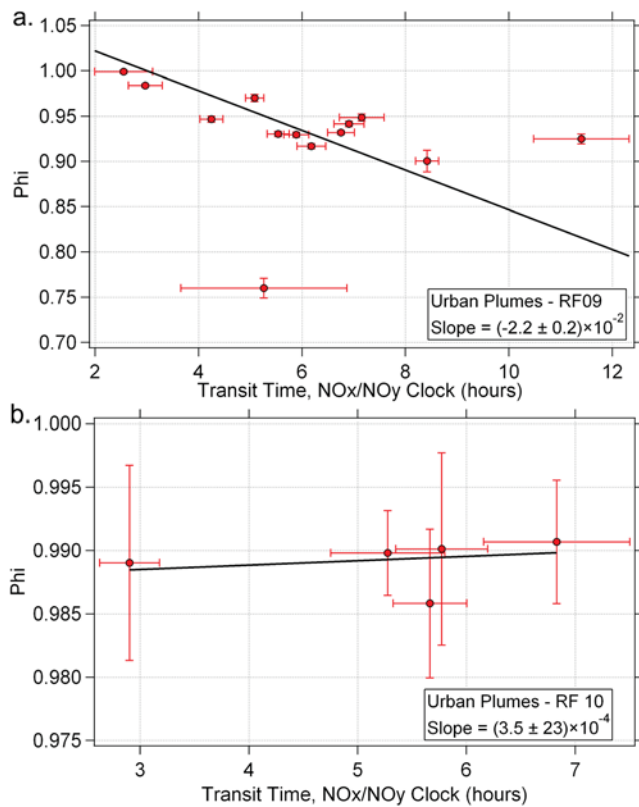


**Figure 10.** Plots for determining the sulfur oxidation rate in urban plumes from nighttime flights research flights (RF) (a) 09 and (b) 10. The transit time uses a  $\text{NO}_x/\text{NO}_y$ -based clock.

of  $\text{SO}_2$ . However, it is consistent with power plant observations, where rapid and nonzero rates were observed for RF 09, while RF 10 rates were indistinguishable from zero.

### 3.4. Observations of Primary Sulfate Emissions From Power Stations

The proximity of many intercepts in the plume source, together with relatively slow oxidation of  $\text{SO}_2$  during the day and night, allowed for the observation of direct emissions of sulfate aerosol or an immediate precursor (e.g.,  $\text{SO}_3$ ) as a percentage of the total sulfur. The distribution of sulfate emissions near or at a power plant, up to 25 km and less than 1 hr of transit time, are presented in the histograms in Figure 11. The left side of Figure 11 shows the number of observations of a given percentage of sulfate during the day and night, which had little or no time for aging after emission. The median percentage of  $\text{SO}_4^{-2}$  from observed plumes was 1.7% and the mean percentage sulfate was 2.8% for all flights.

While outside the 25 km and 1-hr restriction, and several power plant plumes had significant quantities of sulfate, those attributed to either Morgantown or Ft. Martin (Figure 5; RF 09) showed significant quantities in plumes 17 (14.6%), 18 (15.7%), and 19 (17.9%) at night. The Morgantown and Ft. Martin power stations have the same CEMS emission ratio of  $\text{SO}_2/\text{NO}_x$  and cannot be distinguished due to their proximity. These power plants have a CEMS emission ratio of  $\text{SO}_2/\text{NO}_x$  of 0.3 or less, and these measurements were only 40–60 km from Morgantown/Ft. Martin power stations. The plume containing the highest fraction of sulfur was attributed to Harrison Power Plant (Figure S8, RF 12), which showed  $19.8 \pm 0.6\%$  sulfate in plume 10 during the day. This plume intercept, while outside of the 25 km cutoff, was only 28 km away from its source. Most of these levels of sulfate can only be attributed to primary

emissions, and cannot be attributed to  $\text{SO}_2$  oxidation during the winter in the eastern United States. Based on the rate of  $\text{SO}_2$  oxidation determined in this paper, for secondary sulfates in a plume in transport to reach 18% or greater would take 25–82 hr of aging during the day. For the Harrison plant, given a transit time of 1.64 hr, the amount of sulfate being directly emitted would be at least 18.0%.

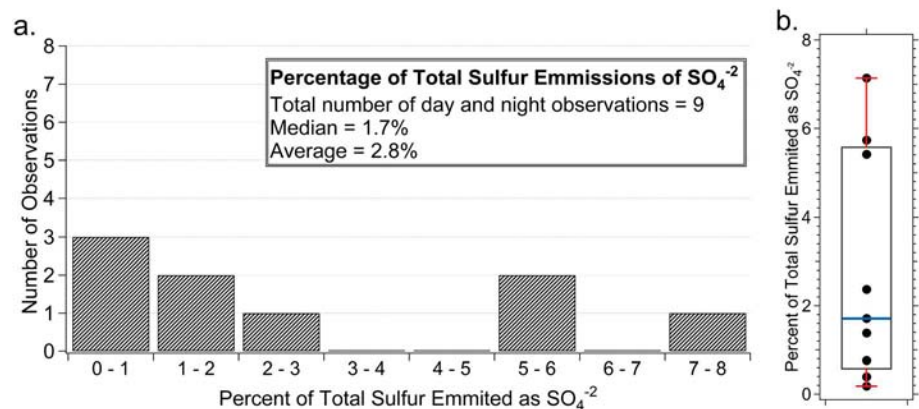


**Figure 11.** (a) Histograms of the fraction of sulfur emission present as sulfate aerosol for night and day flights. (b) A corresponding bar and whisker plot; the median percentage of  $\text{SO}_4^{-2}$  is marked by the blue bar, 25% and 75% by the lower and upper boundary of the box, and the maximum and minimum by the lower and upper red bars. Overlaid on top are the individual points.

#### 4. Conclusions

We report the lifetime and oxidation rate of SO<sub>2</sub> during day and nighttime, in both rural and urban environments, during the WINTER campaign. The daytime conversion rate of SO<sub>2</sub> to SO<sub>4</sub><sup>-2</sup> was 0.22–0.71%/hr, which corresponds to lifetimes of 140–450 hr. Summer time SO<sub>2</sub> oxidation rates previously reported range from 10 to 47 times faster than our wintertime derived values. When clouds are present, aqueous phase oxidation is shown to be very important for SO<sub>2</sub> removal and oxidation by reaction with OH is only a small contribution (Shah et al., 2018). For oxidation by reactions with OH, the daytime SO<sub>2</sub> oxidation rate is a factor of 11.8 slower than NO<sub>2</sub>; hence, NO<sub>2</sub> is expected to be more sensitive to OH than SO<sub>2</sub>. The SO<sub>2</sub> removal rate via OH is expected to be 0.23±0.12%/hr using the relative rate and HNO<sub>3</sub>/NO<sub>y</sub> production rate, which is commensurate with the values derived from the rate of change of the SO<sub>4</sub><sup>-2</sup> to SO<sub>2</sub> ratio. As such, these oxidation rates represent a robust measure of SO<sub>2</sub> oxidation during the winter under cloudless conditions.

Different methods were used to estimate the OH concentration and the subsequent SO<sub>2</sub> removal rate. An upper limit of 9.9 × 10<sup>5</sup> molecules/cm<sup>3</sup> OH was found from HNO<sub>3</sub>/NO<sub>y</sub>. Assuming a first-order process for the production HNO<sub>3</sub> as an alternate measure of OH, an average OH concentration of (1.7±0.3) × 10<sup>5</sup> molecules/cm<sup>3</sup> was found for Homer City and this provides a lifetime of 150±20 hr and 1700±300 hr for NO<sub>2</sub> and SO<sub>2</sub>, respectively. This leads to SO<sub>2</sub> removal rate of 0.058±0.011%/hr, which is slower than the observed lower bound removal rate. Using an estimate of the OH concentration from GEOS-Chem simulations, the predicted an SO<sub>2</sub> removal rate was 0.86–1.1%/hr. GEOS-Chem overestimates OH on average by factor of 2.8 when compared to the NO<sub>x</sub>/NO<sub>y</sub> upper limit. Using OH estimated from measurements of anthropogenic VOCs in urban plumes, OH concentrations were in the range of (-1.2±9.4) × 10<sup>5</sup> molecules/cm<sup>3</sup> and (1.5±3.7) × 10<sup>5</sup> molecules/cm<sup>3</sup>, depending on the AVOC. The most accurate AVOC-based measurement produced removal rates of 0.66±1.63%/hr for NO<sub>x</sub> and 0.054±0.134%/hr for SO<sub>2</sub>. The observed rates of SO<sub>2</sub> removal (0.22–0.71%/hr) is significantly faster than what is expected from AVOC analysis.

Most power plants did not show nighttime removal rates that were different from zero within 1σ, with a removal rate of -0.044±0.077%/hr for Harlee, and +0.61±0.77%/hr for Scherer. Conversion of SO<sub>2</sub> to sulfate in the Conemaugh plume was very fast, at a rate of 2.8±1.7%/hr; some ten times faster than daytime oxidation. However, while its rate was different from zero within 1σ, it was not different from zero within 2σ. This rate is also highly dependent on, and may be an artifact of, the fitting method. Most of the nighttime plumes suggest an oxidation rate of zero. However, Bruce Mansfield shows that a nighttime nonzero removal rate during the winter may be possible. This warrants the investigation of other oxidation mechanisms.

Emissions from urban environments such as Pittsburgh and Atlanta in the nighttime residual layer were explored. Results were mixed. While a significant SO<sub>2</sub> removal rate of 2.2±0.2%/hr for Pittsburgh was measured, the removal rate over Atlanta was not statistically different from zero (+0.035±0.23%/hr).

The total lifetime of SO<sub>2</sub> during the winter depends on rate of daytime and nighttime processing, and the duration of each. The number of hours of daylight varied over the course of the campaign from 10 to 11 hr, so we have assumed an average of 10.5 hr of daylight. If we assume that SO<sub>2</sub> oxidation only occurs during the day and there are no conditions that allow for multiphase chemistry to occur, the lifetime of SO<sub>2</sub> would be 13–43 days, using the range of mean oxidation rates observed for different power plants during the day. When adding the nighttime removal rate from Bruce Mansfield in RF 09 (0.25±0.07%/hr), the SO<sub>2</sub> lifetime shortens to 8.5–21 days. The upper limit of the oxidation rate (the mean+1σ of the fastest day and night observations) is 16.5%/day, corresponding to a lifetime of 6.1 days.

Lastly, primary emissions of sulfate from power plants were observed from intercepts close to their source. The median and mean molar percentages of SO<sub>4</sub><sup>-2</sup> relative to total sulfur (SO<sub>2</sub> + SO<sub>4</sub><sup>-2</sup>) were 1.7 and 2.8%, respectively, for all flights. The largest directly observed value was over 7% sulfate and the largest extrapolated value was 18%.

#### References

- Alexander, B., Park, R. J., Jacob, D. J., & Gong, S. (2009). Transition metal-catalyzed oxidation of atmospheric sulfur: Global implications for the sulfur budget. *Journal of Geophysical Research*, 114, D02309. <https://doi.org/10.1029/2008JD010486>
- Aneja, V. P. (1990). Natural sulfur emissions into the atmosphere. *Journal of the Air & Waste Management Association*, 40(4), 469–476. <https://doi.org/10.1080/10473289.1990.10466701>

#### Acknowledgments

The authors acknowledge the NSF-NCAR Research Aircraft Facility engineers, scientists, pilots, and staff members. Funding for NCAT group participation was made possible by funding from NSF award to Thornton and Jaegle NSF AGS-1360745, and the CU Boulder group is supported by NSF AGS-1360834 and AGS-1822664. EPA Air Markets Program Data are available at <https://ampd.epa.gov/ampd>. Data obtained from the WINTER C-130 research flights used in this study are available at <http://data.eol.ucar.edu/project/WINTER>.



- Apel, E., Hornbrook, R., Hills, A., Blake, N., Barth, M., Weinheimer, A., et al. (2015). Upper tropospheric ozone production from lightning NO<sub>x</sub>-impacted convection: Smoke ingestion case study from the DC3 campaign. *Journal of Geophysical Research: Atmospheres*, 120, 2505–2523. <https://doi.org/10.1002/2014JD022121>
- Atkinson, R., Baulch, D., Cox, R., Crowley, J., Hampson, R., Hynes, R., et al. (2004). Evaluated kinetic and photochemical data for atmospheric chemistry: Volume I-gas phase reactions of Ox, HOx, NO<sub>x</sub> and SO<sub>x</sub> species. *Atmospheric Chemistry and Physics*, 4(6), 1461–1738. <https://doi.org/10.5194/acp-4-1461-2004>
- Bahadori, A. (2011). Estimation of combustion flue gas acid dew point during heat recovery and efficiency gain. *Applied Thermal Engineering*, 31(8–9), 1457–1462. <https://doi.org/10.1016/j.applthermaleng.2011.01.020>
- Bates, T., Lamb, B., Guenther, A., Dignon, J., & Stoiber, R. (1992). Sulfur emissions to the atmosphere from natural sources. *Journal of Atmospheric Chemistry*, 14(1–4), 315–337. <https://doi.org/10.1007/BF00115242>
- Bauer, S., & Koch, D. (2005). Impact of heterogeneous sulfate formation at mineral dust surfaces on aerosol loads and radiative forcing in the Goddard Institute for Space Studies general circulation model. *Journal of Geophysical Research*, 110, D17202. <https://doi.org/10.1029/2005JD005870>
- Behara, S. N., Betha, R., & Balasubramanian, R. (2013). Insights into chemical coupling among acidic gases, ammonia and secondary inorganic aerosols. *Aerosol and Air Quality Research*, 13(4), 1282–1296. <https://doi.org/10.4209/aaqr.2012.11.0328>
- Behra, P., Sigg, L., & Werner, S. (1989). Dominating influence of NH<sub>3</sub> on the oxidation of aqueous SO<sub>2</sub>: The coupling of NH<sub>3</sub> and SO<sub>2</sub> in atmospheric water. *Atmospheric Environment* (1967), 23(12), 2691–2707. [https://doi.org/10.1016/0004-6981\(89\)90549-0](https://doi.org/10.1016/0004-6981(89)90549-0)
- Berndt, T., Jokinen, T., Sipilä, M., Mauldin, R. L., Herrmann, H., Stratmann, F., et al. (2014). H<sub>2</sub>SO<sub>4</sub> formation from the gas-phase reaction of stabilized Criegee intermediates with SO<sub>2</sub>: Influence of water vapour content and temperature. *Atmospheric Environment*, 89, 603–612. <https://doi.org/10.1016/j.atmosenv.2014.02.062>
- Boy, M., Mogensen, D., Smolander, S., Zhou, L., Nieminen, T., Paasonen, P., et al. (2013). Oxidation of SO<sub>2</sub> by stabilized Criegee intermediate (sCI) radicals as a crucial source for atmospheric sulfuric acid concentrations. *Atmospheric Chemistry and Physics*, 13(7), 3865–3879. <https://doi.org/10.5194/acp-13-3865-2013>
- Brown, S. S., An, H., Lee, M., Park, J.-H., Lee, S.-D., Fibiger, D. L., et al. (2017). Cavity enhanced spectroscopy for measurement of nitrogen oxides in the Anthropocene: Results from the Seoul tower during MAPS 2015. *Faraday Discussions*, 200, 529–557. <https://doi.org/10.1039/C7FD00001D>
- Brown, S. S., Dibb, J. E., Stark, H., Aldener, M., Vozella, M., Whitlow, S., et al. (2004). Nighttime removal of NO<sub>x</sub> in the summer marine boundary layer. *Geophysical Research Letters*, 31, L07108. <https://doi.org/10.1029/2004GL019412>
- Brown, S. S., Dubé, W. P., Karamchandani, P., Yarwood, G., Peischl, J., Ryerson, T. B., et al. (2012). Effects of NO<sub>x</sub> control and plume mixing on nighttime chemical processing of plumes from coal-fired power plants. *Journal of Geophysical Research*, 117, D07304. <https://doi.org/10.1029/2011JD016954>
- Brown, S. S., Neuman, J., Ryerson, T., Trainer, M., Dubé, W., Holloway, J., et al. (2006). Nocturnal odd-oxygen budget and its implications for ozone loss in the lower troposphere. *Geophysical Research Letters*, 33, L08801. <https://doi.org/10.1029/2006GL025900>
- Burkholder, J., Sander, J., Abbatt, J., Barker, R., Huie, C., Kolb, et al. (2015). Chemical kinetics and photochemical data for use in atmospheric studies—Evaluation Number 18Rep.
- Cai, C., Hogrefe, C., Katsafados, P., Kallos, G., Beauharnois, M., Schwab, J. J., et al. (2008). Performance evaluation of an air quality forecast modeling system for a summer and winter season—Photochemical oxidants and their precursors. *Atmospheric Environment*, 42(37), 8585–8599. <https://doi.org/10.1016/j.atmosenv.2008.08.029>
- Calvert, J. G., & Stockwell, W. R. (1983). Acid generation in the troposphere by gas-phase chemistry. *Environmental Science & Technology*, 17(9), 428A–443A. <https://doi.org/10.1021/es00115a727>
- Campos, T., Flocke, F., & UCAR/NCAR - Earth Observing Laboratory. (2006). Nitric oxide chemiluminescence ozone instrument for HIAPER. UCAR/NCAR - Earth Observing Laboratory.
- Cao, Y., Zhou, H., Jiang, W., Chen, C.-W., & Pan, W.-P. (2010). Studies of the fate of sulfur trioxide in coal-fired utility boilers based on modified selected condensation methods. *Environmental Science & Technology*, 44(9), 3429–3434. <https://doi.org/10.1021/es903661b>
- Charlson, R. J., Lovelock, J. E., Andreaei, M. O., & Warren, S. G. (1987). Oceanic phytoplankton, atmospheric sulphur, cloud. *Nature*, 326(6114), 655–661. <https://doi.org/10.1038/326655a0>
- Cheng, Y., Zheng, G., Wei, C., Mu, Q., Zheng, B., Wang, Z., et al. (2016). Reactive nitrogen chemistry in aerosol water as a source of sulfate during haze events in China. *Science Advances*, 2(12). <https://doi.org/10.1126/sciadv.1601530>
- Cullis, C., & Hirschler, M. (1980). Atmospheric sulphur: Natural and man-made sources. *Atmospheric Environment* (1967), 14(11), 1263–1278. [https://doi.org/10.1016/0004-6981\(80\)90228-0](https://doi.org/10.1016/0004-6981(80)90228-0)
- Davis, D., Prusaczyk, J., Dwyer, M., & Kim, P. (1974). Stop-flow time-of-flight mass spectrometry kinetics study. Reaction of ozone with nitrogen dioxide and sulfur dioxide. *The Journal of Physical Chemistry*, 78(18), 1775–1779. <https://doi.org/10.1021/j100611a001>
- Day, D. A., Wooldridge, P. J., Dillon, M. B., Thornton, J. A., & Cohen, R. C. (2002). A thermal dissociation laser-induced fluorescence instrument for in situ detection of NO<sub>2</sub>, peroxy nitrates, alkyl nitrates, and HNO<sub>3</sub>. *Journal of Geophysical Research*, 107(D6), 4046. <https://doi.org/10.1029/2001JD000779>
- DeCarlo, P. F., Kimmel, J. R., Trimborn, A., Northway, M. J., Jayne, J. T., Aiken, A. C., et al. (2006). Field-deployable, high-resolution, time-of-flight aerosol mass spectrometer. *Analytical Chemistry*, 78(24), 8281–8289. <https://doi.org/10.1021/ac061249n>
- Dunlea, E., DeCarlo, P., Aiken, A., Kimmel, J., Peltier, R., Weber, R., et al. (2009). Evolution of Asian aerosols during transpacific transport in INTEX-B. *Atmospheric Chemistry and Physics*, 9(19), 7257–7287. <https://doi.org/10.5194/acp-9-7257-2009>
- Fibiger, D. L., McDuffie, E. E., Dubé, W. P., Aiken, K. C., Lopez-Hilfiker, F. D., Lee, B. H., et al. (2018). Wintertime overnight NO<sub>x</sub> removal in a southeastern United States coal-fired power plant plume: A model for understanding winter NO<sub>x</sub> processing and its implications. *Journal of Geophysical Research: Atmospheres*, 123, 1412–1425. <https://doi.org/10.1002/2017JD027768>
- Finlayson-Pitts, B. J., & Pitts, J. N. Jr. (1999). *Chemistry of the upper and lower atmosphere: theory, experiments, and applications*. San Diego, CA: Academic Press.
- Forrest, J., Garber, R. W., & Newman, L. (1981). Onversion rates in power plant plumes based on filter pack data: The coal-fired Cumberland plume. *Atmospheric Environment* (1967), 15(10–11), 2273–2282. [https://doi.org/10.1016/0004-6981\(81\)90259-6](https://doi.org/10.1016/0004-6981(81)90259-6)
- Forrest, J., & Newman, L. (1977). Further studies on the oxidation of sulfur dioxide in coal-fired power plant plumes. *Atmospheric Environment* (1967), 11(5), 465–474. [https://doi.org/10.1016/0004-6981\(77\)90009-9](https://doi.org/10.1016/0004-6981(77)90009-9)
- Fry, J. L., Brown, S. S., Middlebrook, A. M., Edwards, P. M., Campuzano-Jost, P., Day, D. A., et al. (2018). Secondary organic aerosol (SOA) yields from NO<sub>3</sub> radical + isoprene based on nighttime aircraft power plant plume transects. *Atmospheric Chemistry and Physics*, 18(16), 11,663–11,682. <https://doi.org/10.5194/acp-18-11663-2018>

- Gankanda, A., Coddens, E. M., Zhang, Y., Cwiertny, D. M., & Grassian, V. H. (2016). Sulfate formation catalyzed by coal fly ash, mineral dust and iron (iii) oxide: Variable influence of temperature and light. *Environmental Science: Processes & Impacts*, 18(12), 1484–1491. <https://doi.org/10.1039/c6em00430j>
- Garland, J. A. (1977). The dry deposition of sulphur dioxide to land and water surfaces. *Proceedings of the Royal Society of London A*, 354(1678), 245–268. <https://doi.org/10.1098/rspa.1977.0066>
- Guo, H., Weber, R. J., & Nenes, A. (2017). High levels of ammonia do not raise fine particle pH sufficiently to yield nitrogen oxide-dominated sulfate production. *Scientific Reports*, 7(1), 12109. <https://doi.org/10.1038/s41598-017-11704-0>
- Halmer, M., Schmincke, H.-U., & Graf, H.-F. (2002). The annual volcanic gas input into the atmosphere, in particular into the stratosphere: A global data set for the past 100 years. *Journal of Volcanology and Geothermal Research*, 115(3–4), 511–528. [https://doi.org/10.1016/S0377-0273\(01\)00318-3](https://doi.org/10.1016/S0377-0273(01)00318-3)
- Harris, E., Sinha, B., Hoppe, P., Crowley, J., Ono, S., & Foley, S. (2012). Sulfur isotope fractionation during oxidation of sulfur dioxide: Gas-phase oxidation by OH radicals and aqueous oxidation by H<sub>2</sub>O<sub>2</sub>, O<sub>3</sub> and iron catalysis. *Atmospheric Chemistry and Physics*, 12(1), 407–423. <https://doi.org/10.5194/acp-12-407-2012>
- Harris, E., Sinha, B., van Pinxteren, D., Tilgner, A., Fomba, K. W., Schneider, J., et al. (2013). Enhanced role of transition metal ion catalysis during in-cloud oxidation of SO<sub>2</sub>. *Science*, 340(6133), 727–730. <https://doi.org/10.1126/science.1230911>
- Hassler, B., McDonald, B. C., Frost, G. J., Borbon, A., Carslaw, D. C., Civerolo, K., et al. (2016). Analysis of long-term observations of NO<sub>x</sub> and CO in megacities and application to constraining emissions inventories. *Geophysical Research Letters*, 43, 9920–9930. <https://doi.org/10.1002/2016GL069894>
- He, H., Wang, Y., Ma, Q., Ma, J., Chu, B., Ji, D., et al. (2014). Mineral dust and NO<sub>x</sub> promote the conversion of SO<sub>2</sub> to sulfate in heavy pollution days. *Scientific Reports*, 4, 4172.
- Heard, D., Carpenter, L., Creasey, D., Hopkins, J., Lee, J., Lewis, A., et al. (2004). High levels of the hydroxyl radical in the winter urban troposphere. *Geophysical Research Letters*, 31, L18112. <https://doi.org/10.1029/2004GL020544>
- Hoffmann, M. R. (1986). On the kinetics and mechanism of oxidation of aqated sulfur dioxide by ozone. *Atmospheric Environment* (1967), 20(6), 1145–1154. [https://doi.org/10.1016/0004-6981\(86\)90147-2](https://doi.org/10.1016/0004-6981(86)90147-2)
- Holland, F., Hofzumahaus, A., Schäfer, J., Kraus, A., & Pätz, H.-W. (2003). Measurements of OH and HO<sub>2</sub> radical concentrations and photolysis frequencies during BERLIOZ. *Journal of Geophysical Research*, 108(D4), 8246. <https://doi.org/10.1029/2001JD001393>
- Hung, H.-M., & Hoffmann, M. R. (2015). Oxidation of gas-phase SO<sub>2</sub> on the surfaces of acidic microdroplets: Implications for sulfate and sulfate radical anion formation in the atmospheric liquid phase. *Environmental Science & Technology*, 49(23), 13,768–13,776. <https://doi.org/10.1021/acs.est.5b01658>
- Jaeglé, L., Shah, V., Thornton, J. A., Lopez-Hilfiker, F. D., Lee, B. H., McDuffie, E. E., et al. (2018). Nitrogen oxides emissions, chemistry, deposition, and export over the Northeast United States during the WINTER aircraft campaign. *Journal of Geophysical Research: Atmospheres*, 123, 12,368–12,393. <https://doi.org/10.1029/2018JD029133>
- Kenagy, H. S., Sparks, T. L., Ebben, C. J., Wooldridge, P. J., Lopez-Hilfiker, F. D., Lee, B. H., et al. (2018). NO<sub>x</sub> Lifetime and NO<sub>y</sub> partitioning during WINTER. *Journal of Geophysical Research: Atmospheres*, 123, 9813–9827. <https://doi.org/10.1029/2018JD028736>
- Kim, P. S., Jacob, D. J., Fisher, J. A., Travis, K., Yu, K., Zhu, L., et al. (2015). Sources, seasonality, and trends of southeast US aerosol: An integrated analysis of surface, aircraft, and satellite observations with the GEOS-Chem chemical transport model. *Atmospheric Chemistry and Physics*, 15(18), 10,411–10,433. <https://doi.org/10.5194/acp-15-10411-2015>
- Kim, S., Guenther, A., Lefer, B., Flynn, J., Griffin, R., Rutter, A. P., et al. (2015). Potential role of stabilized Criegee radicals in sulfuric acid production in a high biogenic VOC environment. *Environmental Science & Technology*, 49(6), 3383–3391. <https://doi.org/10.1021/es505793t>
- Larssen, T., & Carmichael, G. (2000). Acid rain and acidification in China: The importance of base cation deposition. *Environmental pollution*, 110(1), 89–102. [https://doi.org/10.1016/S0269-7491\(99\)00279-1](https://doi.org/10.1016/S0269-7491(99)00279-1)
- Laursen, K. K., Jorgensen, D. P., Brasseur, G. P., Ustin, S. L., & Huning, J. R. (2006). HIAPER: The next generation NSF/NCAR research aircraft. *Bulletin of the American Meteorological Society*, 87(7), 896–910. <https://doi.org/10.1175/BAMS-87-7-896>
- Lee, B. H., Lopez-Hilfiker, F. D., Mohr, C., Kurtén, T., Worsnop, D. R., & Thornton, J. A. (2014). An iodide-adduct high-resolution time-of-flight chemical-ionization mass spectrometer: Application to atmospheric inorganic and organic compounds. *Environmental Science & Technology*, 48(11), 6309–6317. <https://doi.org/10.1021/es500362a>
- Lee, C., Martin, R. V., van Donkelaar, A., Lee, H., Dickerson, R. R., Hains, J. C., et al. (2011). SO<sub>2</sub> emissions and lifetimes: Estimates from inverse modeling using in situ and global, space-based (SCIAMACHY and OMI) observations. *Journal of Geophysical Research*, 116, D06304. <https://doi.org/10.1029/2010JD014758>
- Lewis, K. A., Arnott, W. P., Moosmüller, H., Chakrabarty, R. K., Carrico, C. M., Kreidenweis, S. M., et al. (2009). Reduction in biomass burning aerosol light absorption upon humidification: roles of inorganically-induced hygroscopicity, particle collapse, and photoacoustic heat and mass transfer. *Atmospheric Chemistry and Physics*, 9(22), 8949–8966. <https://doi.org/10.5194/acp-9-8949-2009>
- Li, G., Bei, N., Cao, J., Huang, R., Wu, J., Feng, T., et al. (2017). A possible pathway for rapid growth of sulfate during haze days in China. *Atmospheric Chemistry and Physics*, 17(5), 3301–3316. <https://doi.org/10.5194/acp-17-3301-2017>
- Li, L., Chen, Z., Zhang, Y. H., Zhu, T., Li, J. L., & Ding, J. (2006). Kinetics and mechanism of heterogeneous oxidation of sulfur dioxide by ozone on surface of calcium carbonate. *Atmospheric Chemistry and Physics*, 6(9), 2453–2464. <https://doi.org/10.5194/acp-6-2453-2006>
- Luria, M., Imhoff, R. E., Valente, R. J., Parkhurst, W. J., & Tanner, R. L. (2001). Rates of conversion of sulfur dioxide to sulfate in a scrubbed power plant plume. *Journal of the Air & Waste Management Association*, 51(10), 1408–1413. <https://doi.org/10.1080/10473289.2001.10464368>
- Manion, J. A., Huie, R. E., Levin, R. D., Burgess Jr, D. R., Orkin, V. L., Tsang, W., et al. (2015). NIST Chemical Kinetics Database, NIST Standard Reference Database 17, Version 7.0 (Web Version), Release 1.6.8, Data version 2015.09, edited, National Institute of Standards and Technology, Gaithersburg, Maryland.
- Martinez, M., Harder, H., Kovacs, T., Simpás, J., Bassis, J., Leshner, R., et al. (2003). OH and HO<sub>2</sub> concentrations, sources, and loss rates during the Southern Oxidants Study in Nashville, Tennessee, summer 1999. *Journal of Geophysical Research*, 108(D19), 4617. <https://doi.org/10.1029/2003JD003551>
- Mauldin III, R. L., Berndt, T., Sipilä, M., Paasonen, P., Petäjä, T., Kim, S., et al. (2012). A new atmospherically relevant oxidant of sulphur dioxide. *Nature*, 488(7410), 193–196. <https://doi.org/10.1038/nature11278>, <https://www.nature.com/articles/nature11278-supplementary-information>
- McDonald, B. C., Gentner, D. R., Goldstein, A. H., & Harley, R. A. (2013). Long-term trends in motor vehicle emissions in US urban areas. *Environmental Science & Technology*, 47(17), 10,022–10,031. <https://doi.org/10.1021/es401034z>

- Middlebrook, A. M., Bahreini, R., Jimenez, J. L., & Canagaratna, M. R. (2012). Evaluation of composition-dependent collection efficiencies for the aerodyne aerosol mass spectrometer using field data. *Aerosol Science and Technology*, 46(3), 258–271. <https://doi.org/10.1080/02786826.2011.620041>
- Park, J., Jang, M., & Yu, Z. (2017). Heterogeneous photo-oxidation of SO<sub>2</sub> in the presence of two different mineral dust particles: Gobi and Arizona dust. *Environmental Science & Technology*, 51(17), 9605–9613. <https://doi.org/10.1021/acs.est.7b00588>
- Parrish, D., Trainer, M., Hereid, D., Williams, E., Olszyna, K., Harley, R., et al. (2002). Decadal change in carbon monoxide to nitrogen oxide ratio in US vehicular emissions. *Journal of Geophysical Research*, 107(D12), 4140. <https://doi.org/10.1029/2001JD000720>
- Pollack, I., Ryerson, T., Trainer, M., Parrish, D., Andrews, A., Atlas, E., et al. (2012). Airborne and ground-based observations of a weekend effect in ozone, precursors, and oxidation products in the California South Coast Air Basin. *Journal of Geophysical Research*, 117(D21), D00V05. <https://doi.org/10.1029/2011JD016772>
- Quan, J., Zhang, X., Zhang, Q., Guo, J., & Vogt, R. D. (2008). Importance of sulfate emission to sulfur deposition at urban and rural sites in China. *Atmospheric Research*, 89(3), 283–288. <https://doi.org/10.1016/j.atmosres.2008.02.015>
- Rattigan, O., Boniface, J., Swartz, E., Davidovits, P., Jayne, J., Kolb, C., & Worsnop, D. (2000). Uptake of gas-phase SO<sub>2</sub> in aqueous sulfuric acid: Oxidation by H<sub>2</sub>O<sub>2</sub>, O<sub>3</sub>, and HONO. *Journal of Geophysical Research*, 105(D23), 29,065–29,078. <https://doi.org/10.1029/2000JD900372>
- Ren, X., Brune, W. H., Mao, J., Mitchell, M. J., Leshner, R. L., Simpas, J. B., et al. (2006). Behavior of OH and HO<sub>2</sub> in the winter atmosphere in New York City. *Atmospheric Environment*, 40, 252–263. <https://doi.org/10.1016/j.atmosenv.2005.11.073>
- Ren, X., Harder, H., Martinez, M., Leshner, R. L., Olliger, A., Simpas, J. B., et al. (2003). OH and HO<sub>2</sub> chemistry in the urban atmosphere of New York City. *Atmospheric Environment*, 37(26), 3639–3651. [https://doi.org/10.1016/S1352-2310\(03\)00459-X](https://doi.org/10.1016/S1352-2310(03)00459-X)
- Roberts, J. M., Hutte, R., Fehsenfeld, F. C., Albritton, D. L., & Sievers, R. E. (1985). Measurements of anthropogenic hydrocarbon concentration ratios in the rural troposphere: Discrimination between background and urban sources. *Atmospheric Environment* (1967), 19(11), 1945–1950. [https://doi.org/10.1016/0004-6981\(85\)90020-4](https://doi.org/10.1016/0004-6981(85)90020-4)
- Ryerson, T., Buhr, M., Frost, G., Goldan, P., Holloway, J., Hübler, G., et al. (1998). Emissions lifetimes and ozone formation in power plant plumes. *Journal of Geophysical Research*, 103(D17), 22,569–22,583. <https://doi.org/10.1029/98JD01620>
- Sakugawa, H., Kaplan, I. R., Tsai, W., & Cohen, Y. (1990). Atmospheric hydrogen peroxide. *Environmental Science & Technology*, 24(10), 1452–1462. <https://doi.org/10.1021/es00080a002>
- Sander, S., Golden, D., Kurylo, M., Moortgat, G., Wine, P., Ravishankara, A., et al. (2006). *Chemical kinetics and photochemical data for use in atmospheric studies evaluation number 15Rep*. Pasadena, CA: Jet Propulsion Laboratory, National Aeronautics and Space Administration.
- Sarwar, G., Fahey, K., Kwok, R., Gilliam, R. C., Roselle, S. J., Mathur, R., et al. (2013). Potential impacts of two SO<sub>2</sub> oxidation pathways on regional sulfate concentrations: Aqueous-phase oxidation by NO<sub>2</sub> and gas-phase oxidation by Stabilized Criegee Intermediates. *Atmospheric Environment*, 68, 186–197. <https://doi.org/10.1016/j.atmosenv.2012.11.036>
- Sarwar, G., Simon, H., Fahey, K., Mathur, R., Goliff, W. S., & Stockwell, W. R. (2014). Impact of sulfur dioxide oxidation by Stabilized Criegee Intermediate on sulfate. *Atmospheric Environment*, 85, 204–214. <https://doi.org/10.1016/j.atmosenv.2013.12.013>
- Schroder, J. C., Campuzano-Jost, P., Day, D. A., Shah, V., Larson, K., Sommers, J. M., et al. (2018). Sources and secondary production of organic aerosols in the northeastern United States during WINTER. *Journal of Geophysical Research: Atmospheres*, 123, 7771–7796. <https://doi.org/10.1029/2018JD028475>
- Shah, V., Jaeglé, L., Thornton, J. A., Lopez-Hilfiker, F. D., Lee, B. H., Schroder, J. C., et al. (2018). Chemical feedbacks weaken the wintertime response of particulate sulfate and nitrate to emissions reductions over the eastern United States. *Proceedings of the National Academy of Sciences*, 115(32), 8110–8115. <https://doi.org/10.1073/pnas.1803295115>
- Shetter, R. E., & Müller, M. (1999). Photolysis frequency measurements using actinic flux spectroradiometry during the PEM-Tropics mission: Instrumentation description and some results. *Journal of Geophysical Research*, 104(D5), 5647–5661. <https://doi.org/10.1029/98JD01381>
- Song, C., M. Phadnis, Q. Carmichael, G. Underwood, T. Miller, E. Balster, and V. Grassian (1970), Modelling heterogeneous reactions in air pollution models, WIT Transactions on Ecology and the Environment, 37.
- Srivastava, R., Miller, C., Erickson, C., & Jambhekar, R. (2004). Emissions of sulfur trioxide from coal-fired power plants. *Journal of the Air & Waste Management Association*, 54(6), 750–762. <https://doi.org/10.1080/10473289.2004.10470943>
- Stevenson, D. S., Johnson, C. E., Collins, W. J., & Derwent, R. G. (2003). The tropospheric sulphur cycle and the role of volcanic SO<sub>2</sub>. *Geological Society, London, Special Publications*, 213(1), 295–305. <https://doi.org/10.1144/GSL.SP.2003.213.01.18>
- Stull, R. B. (1988). *An introduction to boundary layer meteorology*. Dordrecht, The Netherlands: Kluwer Academic.
- Summers, P. W., & Fricke, W. (1989). Atmospheric decay distances and times for sulphur and nitrogen oxides estimated from air and precipitation monitoring in eastern Canada. *Tellus B*, 41(3), 286–295. <https://doi.org/10.3402/tellusb.v41i3.15080>
- Thornton, J. A., Wooldridge, P. J., & Cohen, R. C. (2000). Atmospheric NO<sub>2</sub>: In situ laser-induced fluorescence detection at parts per trillion mixing ratios. *Analytical Chemistry*, 72(3), 528–539. <https://doi.org/10.1021/ac9908905>
- Ullerstam, M., Johnson, M. S., Vogt, R., & Ljungström, E. (2003). DRIFTS and Knudsen cell study of the heterogeneous reactivity of SO<sub>2</sub> and NO<sub>2</sub> on mineral dust. *Atmospheric Chemistry and Physics*, 3(6), 2043–2051. <https://doi.org/10.5194/acp-3-2043-2003>
- Usher, C. R., Al-Hosney, H., Carlos-Cuellar, S., & Grassian, V. H. (2002). A laboratory study of the heterogeneous uptake and oxidation of sulfur dioxide on mineral dust particles. *Journal of Geophysical Research*, 107(D23), 4713. <https://doi.org/10.1029/2002JD002051>
- Wagner, N. L., Riedel, T. P., Young, C. J., Bahreini, R., Brock, C. A., Dubé, W. P., et al. (2013). N<sub>2</sub>O<sub>5</sub> uptake coefficients and nocturnal NO<sub>2</sub> removal rates determined from ambient wintertime measurements. *Journal of Geophysical Research: Atmospheres*, 118, 9331–9350. <https://doi.org/10.1002/jgrd.50653>
- Wallace, H., Jobson, B., Erickson, M., McCoskey, J., VanReken, T., Lamb, B., et al. (2012). Comparison of wintertime CO to NO<sub>x</sub> ratios to MOVES and MOBILE6. 2 on-road emissions inventories. *Atmospheric Environment*, 63, 289–297. <https://doi.org/10.1016/j.atmosenv.2012.08.062>
- Wang, G., Zhang, R., Gomez, M. E., Yang, L., Levy Zamora, M., Hu, M., et al. (2016). Persistent sulfate formation from London Fog to Chinese haze. *Proceedings of the National Academy of Sciences*, 113(48), 13,630–13,635. <https://doi.org/10.1073/pnas.1616540113>
- Weinheimer, A., Walega, J., Ridley, B., Gary, B., Blake, D., Blake, N., et al. (1994). Meridional distributions of NO<sub>x</sub>, NO<sub>y</sub>, and other species in the lower stratosphere and upper troposphere during AASE II. *Geophysical Research Letters*, 21(23), 2583–2586. <https://doi.org/10.1029/94GL01897>
- Welz, O., Savee, J. D., Osborn, D. L., Vasu, S. S., Percival, C. J., Shallcross, D. E., & Taatjes, C. A. (2012). Direct kinetic measurements of Criegee intermediate (CH<sub>2</sub>OO) formed by reaction of CH<sub>2</sub>I with O<sub>2</sub>. *Science*, 335(6065), 204–207. <https://doi.org/10.1126/science.1213229>

- Wild, R. J., Edwards, P. M., Dubé, W. P., Baumann, K., Edgerton, E. S., Quinn, P. K., et al. (2014). A measurement of total reactive nitrogen, NO<sub>y</sub>, together with NO<sub>2</sub>, NO, and O<sub>3</sub> via cavity ring-down spectroscopy. *Environmental Science & Technology*, 48(16), 9609–9615. <https://doi.org/10.1021/es501896w>
- Xie, Y., Ding, A., Nie, W., Mao, H., Qi, X., Huang, X., et al. (2015). Enhanced sulfate formation by nitrogen dioxide: Implications from in situ observations at the SORPES station. *Journal of Geophysical Research: Atmospheres*, 120, 12,679–12,694. <https://doi.org/10.1002/2015JD023607>
- Yamagata, S., Takeshi, K., Takehiko, Z., Naoto, M., Sachio, O., Yasushi, F., et al. (2004). Mineral particles in cloud droplets produced in an Artificial Cloud Experimental System (ACES). *Aerosol Science and Technology*, 38(4), 293–299. <https://doi.org/10.1080/02786820490422871>
- Zaveri, R. A., Berkowitz, C. M., Brechtel, F. J., Gilles, M. K., Hubbe, J. M., Jayne, J. T., et al. (2010). Nighttime chemical evolution of aerosol and trace gases in a power plant plume: Implications for secondary organic nitrate and organosulfate aerosol formation, NO<sub>3</sub> radical chemistry, and N<sub>2</sub>O<sub>5</sub> heterogeneous hydrolysis. *Journal of Geophysical Research*, 115, D12304. <https://doi.org/10.1029/2009JD013250>
- Zhang, Y., & Carmichael, G. R. (1999). The role of mineral aerosol in tropospheric chemistry in East Asia—A model study. *Journal of Applied Meteorology*, 38(3), 353–366. [https://doi.org/10.1175/1520-0450\(1999\)038<0353:TROMAI>2.0.CO;2](https://doi.org/10.1175/1520-0450(1999)038<0353:TROMAI>2.0.CO;2)